

# High energy electromagnetic cascades in extragalactic space: physics and features

V. Berezhinsky<sup>1</sup> and O. Kalashev<sup>2</sup>

<sup>1</sup>*INFN, Gran Sasso Science Institute viale F.Crispi 7, 67100 L'Aquila, Italy and Laboratori Nazionali del Gran Sasso, Assergi (AQ), 67010, Italy*

<sup>2</sup>*Institute for Nuclear Research of the Russian Academy of Sciences, Moscow 117312, Russia*  
(Dated: March 4, 2024)

Using the analytic modeling of the electromagnetic cascades compared with more precise numerical simulations we describe the physical properties of electromagnetic cascades developing in the universe on CMB and EBL background radiations. A cascade is initiated by very high energy photon or electron and the remnant photons at large distance have two-component energy spectrum,  $\propto E^{-2}$  ( $\propto E^{-1.9}$  in numerical simulations) produced at cascade multiplication stage, and  $\propto E^{-3/2}$  from Inverse Compton electron cooling at low energies. The most noticeable property of the cascade spectrum in analytic modeling is 'strong universality', which includes the standard energy spectrum and the energy density of the cascade  $\omega_{\text{cas}}$  as its only numerical parameter. Using numerical simulations of the cascade spectrum and comparing it with recent Fermi LAT spectrum we obtained the upper limit on  $\omega_{\text{cas}}$  stronger than in previous works. The new feature of the analysis is "E<sub>max</sub> rule". We investigate the dependence of  $\omega_{\text{cas}}$  on the distribution of sources, distinguishing two cases of universality: the strong and weak ones.

PACS numbers: 98.70.Sa, 95.85.Pw, 95.85.Ry

## I. INTRODUCTION

Very high energy extragalactic electron or photon colliding with low-energy background photons  $\gamma_t$  (CMB and EBL) produces electromagnetic cascade due to reactions  $\gamma + \gamma_t \rightarrow e^- + e^+$  (pair production, PP) and  $e + \gamma_t \rightarrow \gamma' + e$  (Inverse Compton scattering, IC). Part of the cascade energy can be taken away by synchrotron radiation if magnetic field is strong enough. Existence of such cascading was understood soon after discovery of Cosmic Microwave Background (CMB) radiation [1] and of Greisen-Zatsepin-Kuzmin cutoff [2] (oral remark by I.L. Rozental at Soviet-Union Cosmic Ray Conference, by personal recollection of one of us, VB, and independently by S. Hayakawa according to recollection of K. Sato). Since that time e-m cascading in extragalactic space received many various applications.

One of the earliest applications was rigorous upper limit on cosmogenic neutrino flux, which was proposed by Berezhinsky and Zatsepin in 1969 [3]. The upper limit on this flux as was first obtained in [4] follows from observation that production of neutrinos and initial cascading particles ( $e$  and  $\gamma$ ) takes place from decay of the same particle,  $\Delta^+$  resonance, produced in  $p\gamma_{\text{cmb}}$  interaction, and thus energy density of produced neutrinos and cascade particles are characterised by ratio 1/3. A remarkable byproduct of this work was a good agreement of analytically calculated cascade spectrum with diffuse extragalactic gamma-ray spectrum as presented finally by EGRET collaboration in 1998 [5] in the range from 30 MeV to 130 GeV. The exponent of EGRET spectrum  $\alpha = 2.1 \pm 0.03$  agrees quite well with predicted in [4] as  $\alpha = 2.0$ . The diffuse gamma-ray spectrum measured recently by Fermi-LAT [6, 7] showed much worse agreement with predicted cascade spectrum, in particular the spectrum exponent is found  $\alpha = 2.3$ . The allowed energy

density of the cascade radiation is found [8]

$$\omega_{\text{cas}} = 5.8 \times 10^{-7} \text{ eV/cm}^3, \quad (1)$$

and it puts the severe limit on allowed flux of cosmogenic neutrinos and extragalactic protons in Ultra High Energy Cosmic Rays (UHECR) [8],[9],[10].

The new Fermi data [6] probably contradict also the more general early hypothesis that extragalactic background gamma-ray flux observed by EGRET [5] and Fermi-LAT [6] is fully produced in  $p\gamma$  interaction of extragalactic CRs followed by e-m cascading. This hypothesis, put forward in early 70s e.g. in [11] and [12], had the impact especially on interpretation of the EGRET data, but more complicated Fermi-LAT spectrum and in particular discovery of discrete sources in the early background spectrum seriously questioned this interpretation.

Electromagnetic cascading strongly affected gamma-astronomy of discrete sources. The first work in this field was calculation by Gould and Schreder [13] of absorption of gamma-rays with energies above 100 TeV on CMB radiation in the Universe. Cascading of the absorbed photons was understood soon and in 1970 the absorption of UHE photons on optical, radio-radiation and in magnetic fields were included in the calculations, together with similar calculations for electrons [14].

The new step was done in the work by Aharanian, Coppi and Völk 1994 [15]. Before this work magnetic field in cascading process was taken into account for energy losses of electrons and for absorption of photons in very strong magnetic field. In the work [15] the authors noticed importance of deflection of the cascade electrons in magnetic fields. In absence of magnetic field cascade particles propagate from a source in the same direction as parent photon. If extragalactic magnetic field nearby the source is large enough, the low-energy cascade  $e^+e^-$ -particles can be deflected from the direction

of initial cascading photon and produce (by IC radiation) isotropic low-energy  $E_\gamma < 1$  TeV component named by the authors the “halo component”. As the sources the AGN and in particular blazars are considered. In terms of presently estimated EBL radiation [16], [17] the considered model looks as follows. An initial photon with energy  $E_{\gamma 0} \sim 10$  TeV is absorbed on EBL with the mean absorption length  $\ell_\gamma \sim 100$  Mpc, producing electron and positron with energy  $E_e \sim 5$  TeV each. Electron/positron is deflected in extragalactic magnetic field producing then in IC scattering on a CMB photon the recoil photon with energy

$$E_\gamma^{\text{IC}} \sim (4/3)\gamma_e^2 \epsilon_{\text{cmb}} \sim 100 \text{ GeV} \quad (2)$$

where  $\gamma_e = E_e/m_e$  is the Lorentz-factor of electron. Thus a typical energy of halo radiation is  $E \sim 100$  GeV and the size of halo is  $r_h \sim$  a few Mpc.

A very exiting application of cascading was started by the work of Neronov and Semikoz [18] who indicated a possibility to search for very weak seeds of magnetic fields in the Universe.

Creation of the seeds with extremely weak magnetic fields is a necessary part of explanation of observed magnetic fields which can reach the tremendous values up to  $10^{13}$  G deduced for pulsars. The strong magnetic fields can be produced very fast due to collapse of the objects with weak magnetic field and fast increasing of magnetic fields due to dynamo mechanism. The problem is how the objects with very weak magnetic fields, the seeds, were produced. Two kind of the seeds are in principle known: the cosmological and astrophysical ones (for the reviews see e.g. [19], [20], [21] and latest review with many references [22]). Magnetic seeds of astrophysical origin include historically the first model “Biermann battery” [23], [24] and recently many models based on plasma instabilities e.g. [25] and also on different models for Population III stars, e.g. [26].

To measure magnetic fields in seeds Neronov and Semikoz [18] suggested to observe cascading propagation of TeV gamma-rays from a source through a void with very weak magnetic fields. Secondary positrons and electrons are weakly deflected in magnetic fields producing thus extended emission of IC gamma-rays, i.e. gamma-ray halo described above. Decrease of the size of this halo with energy of emitted gamma-rays allows to measure the strength of magnetic field  $B$  in a range  $10^{-16} \text{ G} \lesssim B \lesssim 10^{-12} \text{ G}$  [27].

At present from observation of cascading radiation of TeV gamma-ray sources (blazars) it became possible to put the lower limit on extragalactic magnetic field [28], for the review and other references see [22].

Following the references cited above and observational data of spectra of TeV blazars obtained by Fermi, one may explain an appearance of lower limit on extragalactic magnetic field in the following way.

Consider first the case  $B = 0$  and gamma-radiation from a blazar with primary energies higher than 1 TeV directed along the jet to an observer. These photons

are absorbed leaving behind the cascade radiation with low-energy spectra  $\propto E^{-2}$  below cutoff and  $E^{-1.5}$  at smaller energies (see [4] and section II). These predicted low-energy spectra exceed the Fermi observation at  $E \sim 1 - 100$  GeV and most natural assumption is suppression of these fluxes due to magnetic field, which deflects  $e^+e^-$  pairs from direction to an observer. The MC simulations from [28, 29] and other calculations cited in [22] result in the lower bound  $B > 10^{-17} \text{ G}$  for extragalactic magnetic fields in voids. All these limits depend on size of coherence length of magnetic field  $\lambda$ .

Apart from lower limits obtained using cascading from different blazars there is one case of the positively measured magnetic field applying quite different method suggested by T. Vachaspati and his collaborators [30],[31] and references therein. This case is relevant for cascading in helical magnetic field. Such field scatters  $e^+e^-$  and provides non-zero correlator between positions of three cascading gamma-quanta produced by IC radiation of electrons and positrons. The data of Fermi from blazars are used for the analysis. The helical magnetic field  $B \sim 10^{-14} \text{ G}$  is found on 10 Mpc scale. This helical magnetic field can be produced in early universe at  $t \sim 1 \text{ ns}$ .

Extragalactic magnetic fields in other structures, like filaments and galaxy clusters are larger by many orders of magnitudes reaching  $\mu\text{G}$  level in clusters. A reader can find more wider and detailed discussion of extragalactic magnetic fields in the review [22]. Above we limited ourselves by several issues connected with cascading.

This paper is organized in the following way. In the section II “Cascade physics and analytic calculations” we describe the cascade physics and obtain analytical solutions of cascade equations.

Our basic model in the section II is a static universe filled by background radiations with dichromatic spectrum of photons with energy  $\epsilon_{\text{cmb}} = 6.3 \times 10^{-4} \text{ eV}$  for CMB and  $\epsilon_{\text{ebl}} = 0.68 \text{ eV}$  for EBL radiation, the only free parameter in this model. Cascade is initiated by very high energy electron or photon with energy  $E_s$  and develops due to pair-production  $\gamma + \gamma_t \rightarrow e^+ + e^-$  and and inverse-compton (IC)  $e + \gamma_t \rightarrow e' + \gamma'$  scattering on background target photons  $\gamma_t$ . At large enough time the spectrum of remnant photons obtains *universal* form (independent from initial energy  $E_s$  assuming  $E_s$  is high enough), which has universal characteristic energies: energy of the spectrum cutoff

$$\mathcal{E}_\gamma^{\text{ebl}} = \frac{m_e^2}{\epsilon_{\text{ebl}}} = 3.9 \times 10^{11} \text{ eV},$$

and energy of spectrum steepening

$$\mathcal{E}_X = \frac{1}{3} \mathcal{E}_\gamma^{\text{ebl}} \frac{\epsilon_{\text{cmb}}}{\epsilon_{\text{ebl}}} = 1.2 \times 10^8 \text{ eV}$$

The spectrum of remnant photons is given by  $n_\gamma(E) \propto E^{-3/2}$  at  $E \leq \mathcal{E}_X$ ,  $n_\gamma(E) \propto E^{-2}$  at  $\mathcal{E}_X \leq E \leq \mathcal{E}_\gamma$ ,  $n_\gamma(E) = 0$  at  $E \geq \mathcal{E}_\gamma$ ,

The spectrum  $n_\gamma(E) \propto E^{-3/2}$  at  $E \leq \mathcal{E}_X$  is robust. The spectrum at  $\mathcal{E}_X \leq E \leq \mathcal{E}_\gamma$  is approximate: numerical simulation give the exponent  $\gamma = 1.9$  instead of 2.0. The cutoff is given in rough approximation.

In subsection IIA we demonstrate that the spectra obtained in static universe using the analytic dichromatic model have the property of universality, which we will later call the strong universality. The main feature of universal spectrum is its fixed shape, independent of initial energy  $E_s$  and distance to the source. The universality is broken for nearby sources.

In subsection IIB the analytic universal spectrum is compared with numerical simulations for the cascades initiated at red-shift  $z$ . For  $z = 0.15$  ( $r=626$  Mpc) agreement for dichromatic model with  $\epsilon_{\text{ebl}} = 0.68$  eV is good, as it is good for larger  $z$  but with choice of different values of  $\epsilon_{\text{ebl}}$ . The case of small distance (low  $z$ ) needs the different treatment.

In subsection IID we consider physically and technically interesting cases of CMB-only radiation. This case is important at large  $z$  when density of CMB photons strongly dominates, and for nearby sources when absorption on EBL is small or absent. Technically the case of CMB-only is interesting because it automatically produces dichromatic effect: the role of EBL photons is played by the photons with energy  $\tilde{\epsilon}_{\text{cmb}}$  from high-energy tail of Planckian distribution whose density is enough to absorb HE cascade photon with energy  $E$  of interest at considered distance  $r$ .

In this approximation we calculated the cascade spectrum from nearby sources  $r=1$  Mpc, 8.5 Mpc, 85 Mpc and 200 Mpc and compared them with numerical simulations also in assumption of CMB-only background radiation. The most noticeable difference with numerical simulation is observed at smallest distance  $r=1$  Mpc because in realistic calculations the cascades arrive to an observer as under-developed with spectrum  $\propto E^{-1.47}$ . The calculated parameters of the cascades are shown in Table I of subsection IIE. The new element of calculations is low-energy suppression of the spectrum shown by  $\mathcal{E}_{\text{lec}}^\gamma$  in Table I.

In the section III we discuss the two numerical simulation techniques for calculation of cascade spectrum, namely solution of one-dimension transport equation and Monte Carlo simulation. The former method is much faster and allows precise calculation of propagated spectra in the case when cascade deflections are not important, while the latter method is good for investigation of the effects of magnetic field, e.g. in a problem of isotropization of the cascades emitted by point sources. We compare our numerically-calculation spectra obtained with two techniques with each other and with independent numerical simulations.

In the section IV the cases of strong and weak universality are introduced and discussed. In section V the corresponding spectra are calculated and compared with that measured by Fermi LAT. This comparison allows to obtain upper limits on energy density of the cascade ra-

diation  $\omega_{\text{cas}}$ , shown in Fig. 11 as function of production redshift. The limits are stronger for generations of the cascades at small redshifts.

In section VI we give a summary of the paper with the main conclusions. This section is written in autonomous way and is destined for a reader who is interested in the main results and wants to bypass the technical details.

We use in the paper the following abbreviations:

UHECR for Ultra High Energy Cosmic Rays, CMB for Cosmic Microwave Background, EBL for Extragalactic Background Light, EGB for Extragalactic Gamma-Ray Background from Fermi-LAT data, IGRB for Isotropic Gamma Ray Background from Fermi-LAT data, IC for Inverse Compton, PP for Pair Production, MC for Monte Carlo, IGMF for Inter Galactic Magnetic Field, MAGIC for Major Atmospheric Gamma Imaging Cherenkov Telescope, H.E.S.S for High Energy Stereoscopic System,

## II. CASCADE PHYSICS AND ANALYTIC CALCULATIONS

We develop here a simplified model for the cascade which allows us to obtain an approximate spectrum of sterile (remnant) photons left behind the cascade multiplication. We perform the approximate calculations of e-m cascade from a burst of radiation in a form of very high energy electrons or photons at very large distance from an observer. One may think of a single electron or photon with very high energy  $E_s \gtrsim 10^{15}$  eV or a number of such particles. We use the *dichromatic spectrum* of background radiation which consists of photons with energy  $\epsilon_{\text{cmb}}$  and  $\epsilon_{\text{ebl}}$ , analogues of cosmic microwave radiation (CMB) and extragalactic background light (EBL) with fixed energies of order of  $6.3 \times 10^{-4}$  eV and  $\sim 1$  eV, respectively. We assume  $\epsilon_{\text{ebl}} \gg \epsilon_{\text{cmb}}$  for energies and  $n_{\text{cmb}} \gg n_{\text{ebl}}$  for space densities. A cascade is initiated by a single electron or photon with very high energy  $E_s$  and proceeds through pair-production (PP),  $\gamma + \gamma_{\text{bckgr}} \rightarrow e^- + e^+$ , and inverse compton (IC) scattering,  $e + \gamma_{\text{bckgr}} \rightarrow e' + \gamma'$ , on low-energy background photons (CMB or EBL). We assume low magnetic field which does not influence the cascade development due to synchrotron radiation, and our calculations will be mostly concerned with the mean diffuse photon flux which is not affected by deflections of the cascade electrons and positrons in the magnetic field.

We consider first the flat static universe and calculate the cascade spectrum from a point-like burst of radiation at a large distance from an observer. The remnant cascade photons at large distances become the cascade-sterile and we refer to spectrum of these photons as universal.

To compare the calculated spectrum with numerical simulations we consider further expanding universe and a burst of high energy radiation at a point with redshift  $z$ . In this case the spectrum of sterile photons remaining

from e-m cascade undergoes the redshift.

### A. Universal spectrum in analytic calculations

In this subsection we consider the flat static universe and e-m cascade from a point-like burst of very high energy photons or electrons at distances from an observer to be large enough for remnant photons to become sterile.

The criterion of high energy (HE) and low energy (LE) for a cascade particle with energy  $E$  is given with help dimensionless parameter  $x_t$

$$x_t = E\varepsilon_t/m_e^2, \quad (3)$$

where  $\varepsilon_t$  is energy of a target photon ( $t=\text{cmb}$  or  $\text{ebl}$ ).  $x_t \gg 1$  and  $x_t \ll 1$  characterizes HE and LE regimes, respectively. In HE regime, for both PP and IC, a cascade particle propagates as a leading particle  $\gamma \rightarrow e \rightarrow \gamma \rightarrow e$  (see Fig. 1, leading-particle regime) losing in each collision (PP and IC) fraction of energy [32]:

$$f \approx 1/[\ln(2E\varepsilon/m_e^2)]. \quad (4)$$

The turning point occurs when a leading particle approaches  $x \gtrsim 1$ , and enters *multiplication regime* II in Fig. 1.

In case of expanding universe we assume that development of the cascade occurs during time  $\tau_{cas}(E)$  much shorter than the Hubble time  $H^{-1}(z_b)$ , where  $\tau_{cas}(E) \sim 1/(\sigma(E)cn_{\text{bckgr}})$  and  $\sigma(E)$  is cross-section for HE photon or electron. The cascade development continues until the cascade photons reach, due to multiplication, the threshold of pair-production in the process  $\gamma + \gamma_{\text{ebl}} \rightarrow e^+ + e^-$ . After this moment the remnant cascade photons loose energy only by redshift.

Because of inequality  $n_{\text{cmb}} \gg n_{\text{ebl}}$  the cascade development proceeds in two stages. At the first one a cascade develops in collisions with CMB photons only:  $\gamma + \gamma_{\text{cmb}} \rightarrow e^- + e^+$  and  $e + \gamma_{\text{cmb}} \rightarrow e' + \gamma'$ . At the second stage the remnant photons from HE part of the distribution are absorbed on EBL radiation  $\gamma + \gamma_{\text{ebl}} \rightarrow e^- + e^+$ , and then the produced  $e^+$  and  $e^-$  are scattered on more numerous CMB photons:  $e + \gamma_{\text{cmb}} \rightarrow e' + \gamma'$ . Because of this, calculations of the cascade on CMB background only, has the physical importance. This stage becomes particularly significant at  $z_b \gg 1$  when the EBL radiation is absent and a cascade develops only on CMB. At smaller redshifts EBL radiation appears, and the cascade enters its second stage.

The remnant photon spectrum is characterized by the following benchmark energies: the minimum energy of absorbed photon  $\mathcal{E}_\gamma^{\text{min}}$ , to which we refer to as *min-photon*, the minimum energy of absorbed photons for CMB background only  $\mathcal{E}_\gamma^{\text{cmb}}$ , minimum energy of the cascade electron/positron  $\mathcal{E}_e = \mathcal{E}_\gamma^{\text{min}}/2$  (*min-electron*) and the energy  $\mathcal{E}_X$  of photon (*X-photon*) produced in IC by min-electron. These energies are listed below in Eq.(5)

together with their numerical values estimated for values  $\epsilon_{\text{cmb}} = 6.3 \times 10^{-4}$  eV and  $\epsilon_{\text{ebl}} = 0.68$  eV (see discussion below).

$$\begin{aligned} \mathcal{E}_\gamma^{\text{min}} &= \mathcal{E}_\gamma^{\text{ebl}} = \frac{m_e^2}{\epsilon_{\text{ebl}}} = 3.9 \times 10^{11} \text{ eV} \\ \mathcal{E}_\gamma^{\text{cmb}} &= \frac{m_e^2}{\epsilon_{\text{cmb}}} = 4.1 \times 10^{14} \text{ eV} \\ \mathcal{E}_e &= \frac{1}{2} \mathcal{E}_\gamma^{\text{min}} = 1.95 \times 10^{11} \text{ eV} \\ \mathcal{E}_X &= \frac{1}{3} \mathcal{E}_\gamma^{\text{min}} \frac{\epsilon_{\text{cmb}}}{\epsilon_{\text{ebl}}} = 1.2 \times 10^8 \text{ eV} \end{aligned} \quad (5)$$

These energies appear in the cascade development illustrated by Fig. 1.

At highest energies  $x \gg 1$  the cascade develops in leading particle regime I,  $\gamma \rightarrow e \rightarrow \gamma \rightarrow e$ , with a small fraction of energy (4) lost in every collision. The non-leading (nl) particle in this process is always electron (or positron). However, as long as  $E_e^{\text{nl}}\varepsilon/m_e^2 \gg 1$  non-leading electron propagates as a leading particle and transfers its energy to cascade multiplication regime II (see Fig. 1, leading-particle regime I). As numerical calculations show, the total energy injected into regime II approximately equals to initial energy  $E_s$ , mainly because the non-leading electrons can enter the multiplication regime (see Fig. 1).

The leading-particle regime finishes at  $\mathcal{E}_\gamma^{\text{cmb}}$ , when  $e^+e^-$  pairs are not produced on CMB photons and approximately at this energy cascade multiplication regime II starts. Pair-production there occurs on EBL radiation while IC proceeds mainly on more numerous CMB photons. The minimum energy  $\mathcal{E}_\gamma^{\text{min}} = 3.9 \times 10^{11}$  eV of photons, which are able to produce  $e^+e^-$  pairs on high-energy EBL target photons, mark the end of the cascade multiplication and beginning of low-energy region III where IC on CMB photons,  $e + \gamma_{\text{cmb}} \rightarrow e' + \gamma'$ , dominates. The produced photons are cascade-sterile and, in consideration of this subsection, propagate not losing the energy adiabatically.

The energy spectrum of these photons is easy to calculate from two relations:  $dn_\gamma = dE_e/E_\gamma$  and  $E_\gamma \approx (E_e/m_e)^2 \epsilon_{\text{cmb}}$ , valid for low-energy regime III. One obtains:

$$dn_\gamma/dE_\gamma \propto E_\gamma^{-3/2} \quad (6)$$

Eq. (6) gives the robust prediction for low-energy asymptotics of the cascade spectrum.

There is one feature common for all stages of the cascade I - III: due to strong dominance of density of CMB photons,  $n_{\text{cmb}} \gg n_{\text{ebl}}$ , IC scattering is always dominated by CMB photons.

For this regime in region III and most part of region II the relation given by equation (7) below is valid:

$$E'_\gamma = \frac{4}{3} \gamma_e^2 \epsilon_{\text{cmb}}, \quad (7)$$



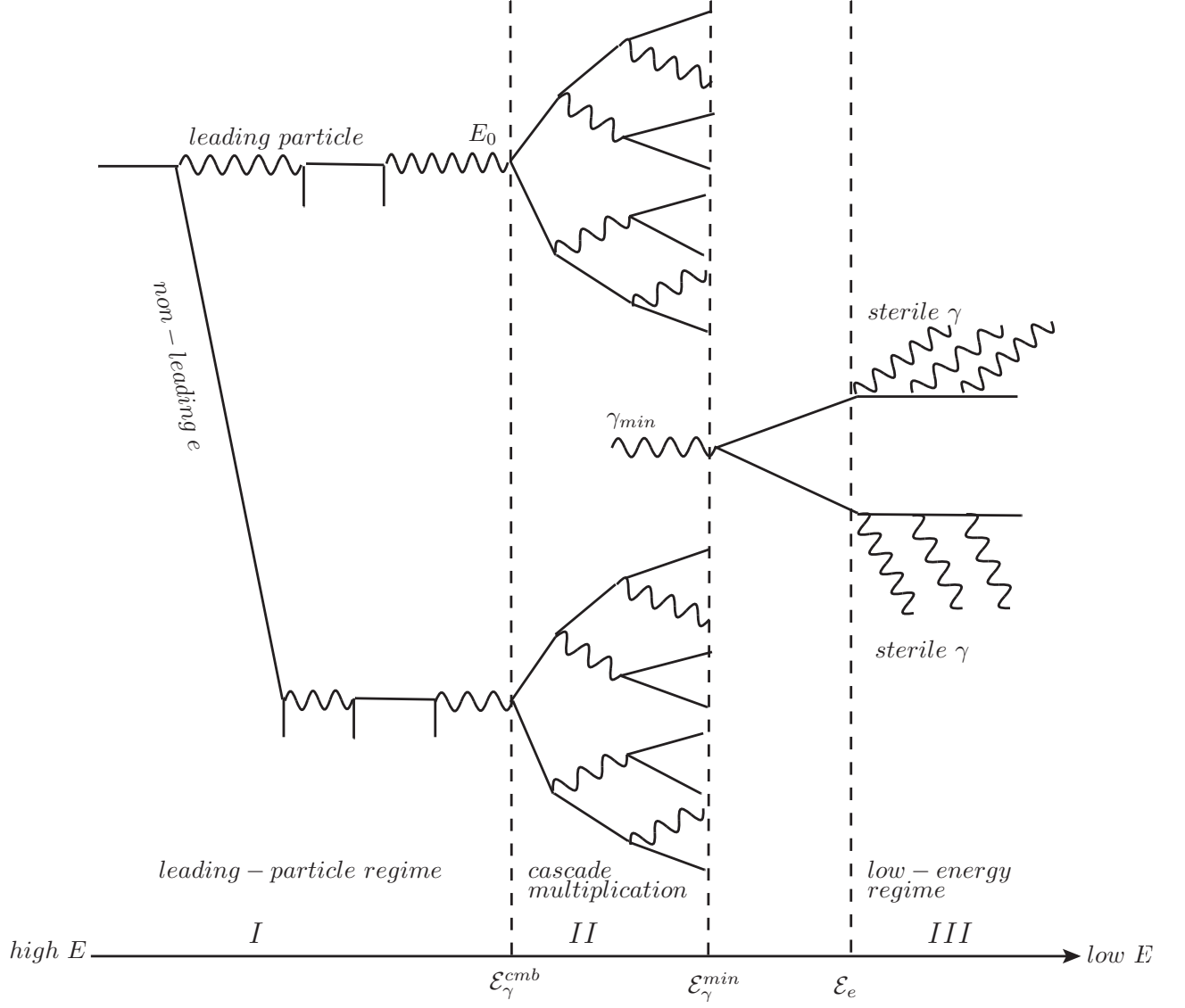


FIG. 1: Qualitative picture of the cascade development in static universe for mono-energetic energies of background photons  $\epsilon_{cmb}$  and  $\epsilon_{ebl}$  with assumption  $\epsilon_{ebl} \gg \epsilon_{cmb}$  and  $n_{cmb} \gg n_{ebl}$ . The energies of cascade particles  $\mathcal{E}_\gamma^{cmb}$ ,  $\mathcal{E}_\gamma^{min}$  and  $\mathcal{E}_e$  mark three regions of the cascade development: (I) HE leading-particle regime when a leading particle losses very small energy in a collision with background photons, (II) fast cascade multiplication, with comparable fraction of energy obtained by each of two produced particles and (III) regime of production of sterile photons by the electrons with energy  $E \leq \mathcal{E}_e$  (see text for the details.)

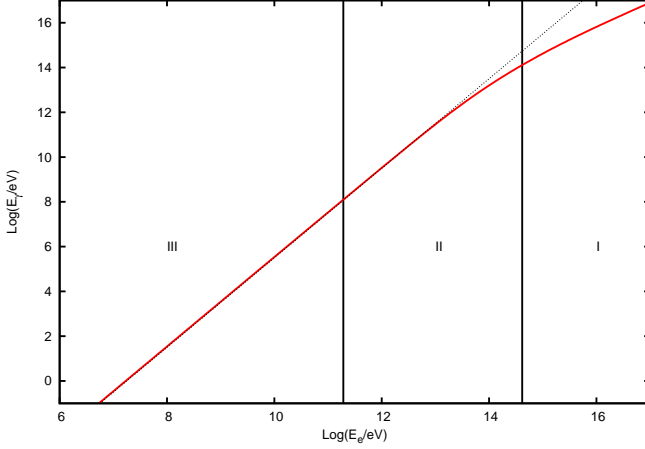


FIG. 2: Comparison of the exact calculation of mean energy of the recoil CMB photon  $E'_\gamma$  in IC scattering (shown by red curve) and its asymptotic dependence according to Eq. (7) (black dotted line).

where  $\gamma_e = E_e/m_e$  is the electron Lorentz-factor and  $E'_\gamma$  is the average energy of cmb photon after scattering off the electron. This equation was obtained in [33] and [32] and it is valid at energy of target photons  $\varepsilon_r \ll m_e$  in the system where the electron is at rest.

The essential feature of Eq.(7),  $E'_\gamma \sim \gamma_e^2 \epsilon_{\text{cmb}}$  can be easily obtained from the Lorentz transformations. Indeed, consider an electron with Lorentz factor  $\gamma_e$  colliding with CMB photon  $\epsilon_{\text{cmb}}$ . The energy of this target photon in the system of electron at rest,  $\epsilon_r \sim \gamma_e \epsilon_{\text{cmb}}$  is assumed to be much smaller than  $m_e$ . After scattering such photon does not change its energy  $\epsilon'_r = \epsilon_r$ , and in laboratory system it is typically boosted by another Lorentz factor  $\gamma_e$ :  $\epsilon' \sim \gamma_e \epsilon'_r \sim \gamma_e^2 \epsilon_{\text{cmb}}$ . In Fig. 2 we compare  $E'_\gamma$  from Eq. (7) (black dotted line) with exact calculation (red line) both given as a function of electron energy  $E_e$  plotted at abscissa. One may see that maximum energy  $E'_\gamma$  from Eq. (7) is valid up to  $3 \times 10^{13}$  eV. In fact in all cases of applications below the maximum energy of photon spectra is provided by absorption on EBL radiation and thus maximum energy is given by  $\mathcal{E}_\gamma^{\text{ebl}} = \frac{m_e^2}{\epsilon_{\text{ebl}}} = 3.9 \times 10^{11}$  eV, much below  $3 \times 10^{13}$  eV allowed by exact calculations. The only almost exceptional case  $\mathcal{E}_X = 2.0 \times 10^{13}$  eV is given by nearby sources (see Table I in Section II E). Probably too flat  $\propto E^{-1.7}$  part of the spectrum between  $\mathcal{E}_X$  and  $\mathcal{E}_\gamma$  is a reflection of more flat red curve in Fig. 2 above  $E'_\gamma = 3 \times 10^{13}$  eV.

It is important to note that instead of following the time-dependent cascade development, we consider a history of a cascade in terms of *particle generations*. Particles, electrons and photons, can reach given generation  $\nu$  at different times. The total number of particles in one generation is  $N_{\text{tot}} = 2^\nu$  and relation between number of electrons  $N_e$  and photons  $N_\gamma$  in the same generation with large  $\nu$  is approximately  $N_e \approx 2N_\gamma$  (in case a cas-

cade starts by electron this relation is given by  $N_e = 2N_\gamma + (-1)^\nu$  and in case by photon  $N_e = 2N_\gamma - 2(-1)^\nu$ ).

For calculation of the cascade energy spectrum we introduce the quantity  $q(E)$ , as a number of cascade particles passing through energy  $E$  during the whole time of cascade propagation. For electrons and photons we use notation  $q_e(E)$  and  $q_\gamma(E)$ , respectively. Assuming that total energy in the cascade is conserved, one can use the equality of primary-particle energy  $E_s$  and the total energy  $E \times q(E)$  which flows through energy  $E$  during all cascade history. Taking into account that  $N_e \approx 2N_\gamma$  in each generation of the cascade in the multiplication region II, one obtains  $q_e(E) = (2/3)E_s/E$  and  $q_\gamma(E) = (1/3)E_s/E$  (for different way to prove  $q(E) \propto (1/E)$  see [4] and [34]). For low-energy regime III we have  $q_e(E) = \text{const}$  for electrons and  $q_\gamma(E)$  increasing with energy due to low-energy tail of photons produced by electrons.

The basic equation for the number of the cascade photons  $n_\gamma(E)$  reads

$$dn_\gamma(E_\gamma) = q_e(E_e) dE_e / E_\gamma. \quad (8)$$

In low-energy regime III we can use additionally to Eq. (8)  $q_e(E_e) = q_0$  at  $E_e \leq \mathcal{E}_e$ , and  $E_\gamma \propto E_e^2$  for IC photon production on CMB photons. It results in  $dn_\gamma/dE_\gamma \propto E_\gamma^{-3/2}$  at  $E_\gamma \leq \mathcal{E}_X$  in agreement with Eq. (6).

In multiplication regime II we use additionally to basic equation (8),  $q_e(E_e) \propto 1/E_e$  and  $E_\gamma \propto E_e^2$ . We obtain thus  $dn_\gamma/dE_\gamma \propto E_\gamma^{-2}$ , valid in the interval  $\mathcal{E}_X \leq E_\gamma \leq \mathcal{E}_\gamma^{\text{min}}$ . At  $E_\gamma \geq \mathcal{E}_\gamma^{\text{min}}$  all remnant photons are absorbed and  $dn_\gamma/dE_\gamma = 0$ .

Thus we finally obtain for the spectrum of remnant photons in terms of the total number of particles  $n_\gamma$ :

$$n_\gamma(E_\gamma) = \begin{cases} (K/\mathcal{E}_X)(E_\gamma/\mathcal{E}_X)^{-3/2} & \text{at } E_\gamma \leq \mathcal{E}_X \\ (K/\mathcal{E}_X)(E_\gamma/\mathcal{E}_X)^{-2} & \text{at } \mathcal{E}_X \leq E_\gamma \leq \mathcal{E}_\gamma \\ 0 & \text{at } E_\gamma > \mathcal{E}_\gamma \end{cases} \quad (9)$$

where absorption energy  $\mathcal{E}_\gamma = \mathcal{E}_\gamma^{\text{min}} = m_e^2/\epsilon_{\text{ebl}} = 3.9 \times 10^{11}$  eV, is minimum energy of absorbed photon (min-photon), and transition energy  $\mathcal{E}_X = (4/3)(\mathcal{E}_e/m_e)^2 \epsilon_{\text{cmb}} = 1.2 \times 10^8$  eV is the energy of IC photon radiated by min-electron produced in absorption of min-photon. Everywhere below we use  $\mathcal{E}_\gamma$  and  $\mathcal{E}_X$  as generic notation for cutoff energy and energy of transition between  $E^{-3/2}$  and  $E^{-2}$  regimes, respectively. The background radiation (cmb or ebl) can be indicated as indices, when it is needed. The normalizing coefficient  $K$  can be found from conservation of energy in the cascade, with the total energy equals to energy  $E_s$  of primary electron or photon.

$$K = \frac{E_s}{\mathcal{E}_X(2 + \ln \mathcal{E}_\gamma/\mathcal{E}_X)}. \quad (10)$$

We will refer to spectrum (9) with normalization (10) as *universal spectrum*: its shape is fixed independently on initial energy  $E_s$  or even injection spectrum  $Q(E_s)$ , if

initial energy is sufficiently high, larger than scale energy  $E_0$ , which can be taken as  $\mathcal{E}_\gamma^{\text{cmb}}$  from Eq. (5).

The initial energy  $E_s$  (or energy density  $\omega_{\text{cas}}$  for diffuse flux) changes only total normalization coefficient  $K$  from Eq. (10). Thus the shape of the cascade spectrum does not depend on the injection spectrum and propagation time (spectrum is frozen at the remnant-photons stage and forgets about its production stage). This universality will be referred to as 'strong universality'.

The universal spectrum given by Eq. (9) with normalization (10) has been obtained above in the simple model for static flat universe, but in fact it is valid for a wide class of different models, e.g. for realistic expanding universe at fixed redshift, if cascade develops at time  $\tau$  shorter than the Hubble time  $H^{-1}(z)$ . In many cases below, Eqs (9) and (10) are valid, though with numerical values of  $\mathcal{E}_\gamma$ ,  $\mathcal{E}_X$  and  $K$  different from that given above.

The universal spectrum of remnant photons left behind cascading of particles on dichromatic background photons with energies  $\varepsilon_{\text{cmb}} = 6.3 \times 10^{-4}$  eV and  $\varepsilon_{\text{ebl}} = 0.68$  eV in flat universe at large distance from an observer is characterized by the following spectral features: it has a flat energy spectrum  $\propto E_\gamma^{-3/2}$  from the lowest energies and up to  $\mathcal{E}_X = 1.2 \times 10^8$  eV; it becomes more steep  $\propto E^{-2}$  at higher energies, followed by a sharp cut-off at  $\mathcal{E}_\gamma = m_e^2/\varepsilon_{\text{ebl}} = 3.9 \times 10^{11}$  eV due to absorption on EBL photons. The most reliable predictions of this simple model are low energy spectral shape  $\propto E^{-3/2}$  (robust) and cascade-multiplication one  $\propto E^{-2}$  (probably approximate), while prediction of sharp cutoff at  $\mathcal{E}_\gamma$  is caused by assumption of large distance to the source and monochromatic spectrum of EBL. The sharpness of the spectral feature at  $\mathcal{E}_X$  with its numerical value is artifact of dichromatic model of background radiation. In fact at both energies  $\mathcal{E}_X$  and  $\mathcal{E}_\gamma$  there must be the transition regions.

The low-energy component of spectrum (9)  $\propto E^{-1.5}$  is a signature of low-energy IC scattering (7), while the component  $\propto E^{-2}$  is a signature of the cascade multiplication (region II in Fig. 1 up to cutoff at energy  $\mathcal{E}_\gamma^{\text{ebl}} = 3.9 \times 10^{11}$  eV).

Eq. (9) gives the total number of photons from a point-like source. In particular in case of one primary UHE photon/electron  $n_\gamma(E_\gamma)dE_\gamma$  gives the total number of the cascade photons with energy  $E_\gamma$  observed at any large distance  $r$  from a source. Since the both characteristic energies  $\mathcal{E}_\gamma$  and  $\mathcal{E}_X$  do not depend on distance and energy  $E_s$ , Eq. (9) presents the same universal spectrum  $n_\gamma(E_\gamma)$  for any initial energy  $E_s$  being larger than energy  $\mathcal{E}_\gamma$ . Eq. (9) gives also *diffuse flux* with normalization  $E_s$  substituted by the energy density of the cascade radiation  $\omega_{\text{cas}}$ . Since the cascade spectra  $n_\gamma(E_\gamma)$  are the same far all  $E_s$  (apart from the total normalization) the spectra are the same for any generation spectrum  $Q_g(E_s)$ . In other words the resultant universal spectrum forgets about its parent generation spectrum.

The *diffuse flux* of the cascade radiation is described by the space density of the cascade photons  $n_\gamma(E_\gamma)$  with

normalization given by Eq. (10) where  $E_s$  is substituted by the energy density  $\omega_{\text{cas}}$ . The problem here is an additional component at  $E_\gamma > \mathcal{E}_\gamma$  due to nearby sources (see subsection IIE).

In conclusion, the universality of spectrum (9) for both remote point-like sources and diffuse radiation implies that all characteristics of the spectrum do not depend on the primary energy  $E_s$  and distance  $r$  (for a point-like source). The universal spectrum, obtained above in a static universe, describes in fact rather wide class of remote gamma-ray sources in the universe and also diffuse gamma-ray radiation. In the next subsections IIB, IIC and IIE we will present the relevant comparison with numerical simulations for point-like sources and discuss the phenomena which limit the validity of the universal spectrum.

## B. Comparison of universal spectrum with numerical simulations

In this subsection we compare the universal spectrum, obtained within our simplified model, with realistic numerical simulation. Universal spectrum (9) is not valid for sources at too small and too large redshifts  $z$ . At small redshifts (nearby sources) absorption on EBL, which is essential feature of our model, may not occur because of small distance and low space density of EBL photons. Cascades may not be produced at all if a primary photon has energy  $E_s$  less than threshold of pair production on EBL,  $\mathcal{E}_\gamma$ .

Note that in our calculations we did not include at all the density of target photons. Instead we just assumed that distance to a source is large enough for photon absorption at  $E > \mathcal{E}_\gamma$ .

For nearby sources this assumption fails. In case of low density  $n_{\text{ebl}}$  of EBL photons,  $\sigma_{\text{pair}}n_{\text{ebl}}r_{\text{source}} \ll 1$ , cascade may still develop on CMB only; and this case will be considered below. Even if a photon is absorbed, cascade still may not develop. It happens when characteristic IC radiation length for secondary electron/positron exceeds the distance to the observer.

At the large redshifts  $z$  comparison with numerical simulations may fail, because in analytic calculations we neglect effects of the universe expansion and energy redshift. We will include these effects in the next subsection and thus extend our consideration to larger redshifts. The first comparison of analytic calculations [36] (similar to our static-universe model) with MC simulation for sources with fixed redshift  $z$  was done in [35] and presented in the upper panel of Fig. 3. We can compare now the predicted spectrum (9) shown by thick black line, with MC spectrum from [35]. For  $z = 0.15$  ( $r = 626$  Mpc) we see the good agreement with the model where energy of EBL photons are fixed as  $\varepsilon_{\text{ebl}} = 0.676$  eV. The low-energy spectrum  $\propto E^{-1.5}$  is reliably confirmed. The cascade multiplication spectrum ( $\propto E^{-2}$ ) is seen as  $E^{-1.9}$ . Values of  $\mathcal{E}_X$  and  $\mathcal{E}_\gamma$

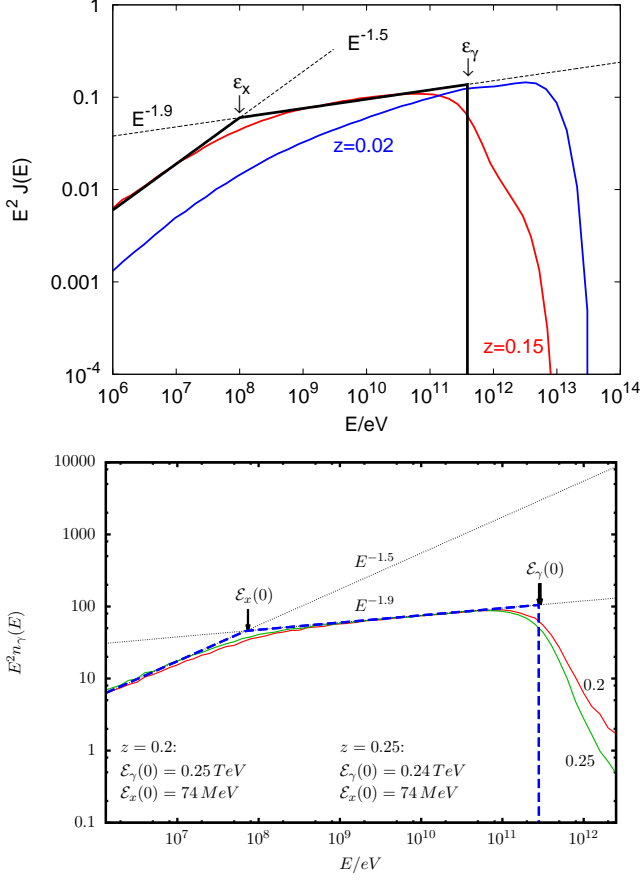


FIG. 3: Comparison of analytic calculations (black thick line) with numerical simulation (red and blue lines) for  $z = 0.15$  and  $z = 0.02$  correspondingly from the work by Kachelrieß et al [35] (*upper panel*) and from the present work (*lower panel*) for redshifts  $z = 0.2$  (red line) and  $0.25$  (green line). Analytic calculations in the lower panel are presented by blue broken lines. For the both panels the line  $\propto E^{-1.5}$  is shown for comparison; the characteristic energies in analytic calculations  $\mathcal{E}_X$  and  $\mathcal{E}_\gamma$  are shown by arrows (see the text).

agree well with MC simulation. The MC simulation gives a smooth transition between different regimes, while in analytic calculations it is sharp because of dichromatic spectrum of background.

For  $z = 0.02$  ( $r = 83.4 \text{ Mpc}$ ) agreement is bad and it has to be interpreted as small distance to the source.

In the lower panel of Fig. 3 the analytic spectrum (9) is compared with our numerical simulations with the same conclusions (see subsection III).

The success of static model is provided by large, but not too large value of  $z$ . For larger redshifts we have to generalize our analytic calculations for expanding universe.

### C. Expanding universe and comparison for $z > 0.3$

For large redshifts  $z > 0.3$  we assume that cascades have enough time to be developed during the Hubble time  $H^{-1}(z)$  to the spectrum given by Eq. (9). The energies of background photons at epoch  $z$  are assumed to be  $\varepsilon_{\text{cmb}}(z) = (1+z)\varepsilon_{\text{cmb}}$  for CMB and  $\varepsilon_{\text{ebl}}^z > \varepsilon_{\text{ebl}}$  for EBL. Accordingly, the characteristic energies at redshift  $z$  become  $\mathcal{E}_\gamma(z) = m_e^2/\varepsilon_{\text{ebl}}^z$  and  $\mathcal{E}_X(z) = \frac{1}{3}(\mathcal{E}_\gamma(z)/m_e)^2\varepsilon_{\text{cmb}}(z)$ . Spectrum of remnant photons at epoch  $z$ ,  $n_\gamma(E_\gamma, z)$ , is given by Eq. (9) with  $\mathcal{E}_X \equiv \mathcal{E}_X(z)$  and  $\mathcal{E}_\gamma \equiv \mathcal{E}_\gamma(z)$ . At propagation of this spectrum to  $z = 0$ , the energies of photons  $E_\gamma$  and characteristic energies  $\mathcal{E}_\gamma(z)$  and  $\mathcal{E}_X(z)$  are redshifted by factor  $(1+z)$ , but Eq. (9) remains the same with invariant value of  $K$  provided by conservation of number of particles during the redshift process,  $n_\gamma(E_\gamma, z)dE_\gamma = n_\gamma(E, 0)dE$ . Redshifted characteristic energies are given by

$$\mathcal{E}_\gamma(0) = \frac{m_e^2}{\varepsilon_{\text{ebl}}^z} \frac{1}{1+z}, \quad \mathcal{E}_X(0) = \frac{m_e^2 \varepsilon_{\text{cmb}}}{3(\varepsilon_{\text{ebl}}^z)^2}. \quad (11)$$

From the second relation in Eq. (11) one finds the energy of EBL photon  $\varepsilon_{\text{ebl}}^z$  at epoch  $z$  as

$$\varepsilon_{\text{ebl}}^z = \left( \frac{m_e^2 \varepsilon_{\text{cmb}}}{3\mathcal{E}_X(0)} \right)^{1/2}. \quad (12)$$

Now the procedure of comparing of analytic solution with numerical simulation consists of the the following four operations illustrated by Fig. 4:

- (i) Normalization of  $E^{-1.5}$  part of analytic solution by  $E^{-1.5}$  part of the simulation.
- (ii) Finding  $\mathcal{E}_X(0)$  as intersection of  $E^{-1.5}$  and  $E^{-1.9}$  parts of the spectrum (see Fig. 4). In this operation we neglect the difference between  $E^{-1.9}$  and  $E^{-2}$ .
- (iii) Calculation of  $\varepsilon_{\text{ebl}}^z$  using Eq. (12).
- (iv) Calculation of cutoff energy  $\mathcal{E}_\gamma(0)$  from Eq. (11).

Comparison of analytic solutions with numerical simulation is presented in Fig. 4 for redshifts  $z = 0.32, 0.4, 0.64, 1.0$ . The analytic solution predicts that cascade spectrum consists of two power-law components  $E^{-1.5}$  and  $E^{-2}$ , with intersection at  $\mathcal{E}_X$ . The numerical simulations confirm this prediction with component  $E^{-1.9}$  instead of  $E^{-2}$ . The only free parameter in analytic calculations is energy of EBL photons for each redshift, which means the value of  $\varepsilon_{\text{ebl}} \approx 0.68$  at  $z = 0$  and evolution  $\varepsilon_{\text{ebl}}^z/\varepsilon_{\text{ebl}} = f(z)$ . Free parameter  $\varepsilon_{\text{ebl}}^z$  determines two characteristic energies  $\mathcal{E}_X$  and  $\mathcal{E}_\gamma$ .

In contrast to the sharp spectral features in analytic calculations, the numerical simulations predict a smooth transition regimes centered by these features.

The evolution of EBL energy  $\varepsilon_{\text{ebl}}^z/\varepsilon_{\text{ebl}}$  with  $z$  in dichromatic model must correspond, to some extent, to the evolution of the mean EBL energy  $\bar{\varepsilon}_{\text{ebl}}(z)$  with redshift.

The numerical simulations show an interesting feature of merging the spectrum  $n_\gamma(E, z)$  to  $E^{-1.9}$  at increasing  $z$ , which coincides within accuracy of calculations with



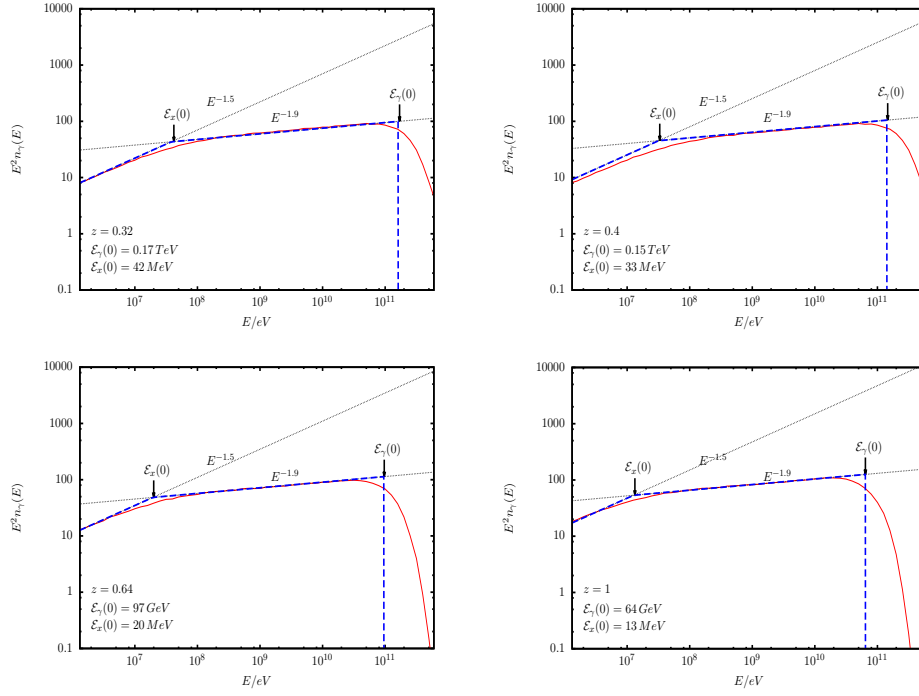


FIG. 4: Comparison of analytic calculations with numerical simulations from this work for large redshifts  $z > 0.3$ . Four panels show the comparison for redshifts 0.32, 0.4, 0.64, and 1.0 with the same notation as in Fig. 3 (see the text for details).

fundamental spectrum of the cascade multiplication  $E^{-2}$  in analytic calculations (see Fig. 5).

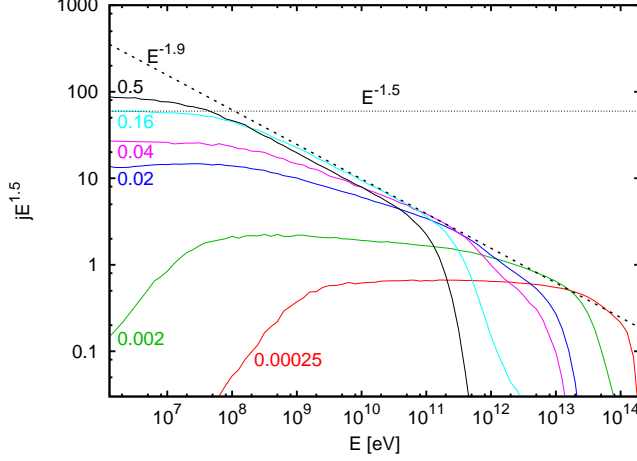


FIG. 5: Merging at increasing  $z$  of numerically-simulated spectra to the universal  $E^{-1.9}$  spectrum, which within accuracy of calculations coincides with fundamental cascade-multiplication spectrum  $\propto E^{-2}$  in analytic calculations.

#### D. Cascading only on CMB

This section has a technical character. Study of the cascade development only on CMB is important at least in two cases discussed in this paper:

(i) In the case of nearby sources when absorption of photons on EBL is absent.

(ii) In expanding universe at large redshifts, when due to high space density of CMB photons a cascade is developing very fast with cutoff at  $\mathcal{E}_\gamma^{\text{cmb}} = m_e^2/\varepsilon_{\text{cmb}}^z$ . Only later the HE tail of the cascade photon distribution is slowly absorbed on EBL, followed by IC of produced electrons and positrons on CMB photons.

Consider first cascading on *monochromatic CMB* at  $z = 0$ . The energy spectrum of cascade is given again by Eq. (9) with

$$\mathcal{E}_\gamma = \mathcal{E}_\gamma^{\text{cmb}} = m_e^2/\varepsilon_{\text{cmb}} \approx 4.1 \times 10^{14} \text{ eV} \quad (13)$$

and

$$\mathcal{E}_X = (4/3)(\mathcal{E}_e/m_e)^2 \varepsilon_{\text{cmb}} = (1/3)\mathcal{E}_\gamma^{\text{cmb}} \quad (14)$$

The normalization is given by the same equation (10) with  $\mathcal{E}_\gamma/\mathcal{E}_X = 3$  as follows from Eq. (14).

The remarkable feature of this calculation is prediction of very narrow cascade-multiplication energy width given by ratio  $\mathcal{E}_\gamma/\mathcal{E}_X = 3$ , to be compared with  $3 \times 10^3$  for universal spectrum (9). This is the direct consequence of monochromatic CMB model accepted here (see discussion in the end of this subsection).

For redshift  $z$  there are two spectra of interest: the equilibrium spectrum at epoch  $z$ ,  $n_\gamma(E_\gamma, z)$ , and this spectrum redshifted to epoch  $z = 0$ ,  $n_\gamma(E, 0)$ .

Consider first the former. It is given by Eq. (9) with  $\varepsilon_{\text{cmb}}^z = \varepsilon_{\text{cmb}}(1+z)$  and by characteristic energies at epoch  $z$  as

$$\mathcal{E}_\gamma(z) = m_e^2/\varepsilon_{\text{cmb}}^z, \quad \mathcal{E}_X(z) = (1/3)\mathcal{E}_\gamma(z). \quad (15)$$

The normalization is given by Eq. (10) with  $\mathcal{E}_\gamma(z)/\mathcal{E}_X(z) = 3$ .

The spectrum redshifted to  $z = 0$  may be also of interest for applications. It is given by redshifted characteristic energies  $\mathcal{E}_\gamma(0) = \mathcal{E}_\gamma(z)/(1+z)$  and  $\mathcal{E}_X(0) = \mathcal{E}_X(z)/(1+z)$ :

$$\mathcal{E}_\gamma(0) = \frac{m_e^2}{\varepsilon_{\text{cmb}}(1+z)^2} \quad (16)$$

and

$$\mathcal{E}_X(0) = (1/3)\mathcal{E}_\gamma(0) = (1/3)\frac{m_e^2}{\varepsilon_{\text{cmb}}(1+z)^2} \quad (17)$$

The redshift leaves constant  $K$  in normalization (10) invariant.

In fact, the monochromatic CMB model considered above is unrealistic and introduction of dichromatic model is necessary in most applications. It can be explained for example by cascading on CMB at  $z = 0$  at distance  $r$  from an observer. IC scattering occurs on all CMB photons which energy can be assumed as  $\varepsilon_{\text{cmb}} = 6.3 \times 10^{-4} \text{ eV}$ . However, absorption of photons occurs on CMB photons from high energy tail of Planckian distribution and minimum energy of absorbed photons  $\tilde{\mathcal{E}}_{\text{min}}$  is determined by much higher energies of CMB photons  $\tilde{\varepsilon}_{\text{cmb}} \gg \varepsilon_{\text{cmb}}$  as

$$\tilde{\mathcal{E}}_{\text{min}} = \tilde{\varepsilon}_{\text{min}}^{\text{cmb}} = m_e^2/\tilde{\varepsilon}_{\text{cmb}}. \quad (18)$$

Energy  $\tilde{\varepsilon}_{\text{cmb}}$  coincides with minimum energy in HE tail of CMB photons for given  $E_\gamma$  because with increasing of  $\varepsilon$  the number density of CMB photons exponentially falls down.

Therefore, we come back to the standard spectrum given by Eq (9) distorted at the highest energies due to distortion of relation  $E_\gamma = \frac{4}{3}\gamma_e^2 \varepsilon_{\text{cmb}}$  and with  $\varepsilon_{\text{eb1}}$  substituted everywhere by  $\tilde{\varepsilon}_{\text{cmb}}$ .

#### E. Cascades from nearby sources

In this section we calculate the cascade spectrum taking into account only CMB radiation and compare them with numerical calculations at the same assumptions. This procedure clarifies the interesting physical details. As argued above the cascade spectrum on CMB-only must be calculated using the dichromatic model of background radiation with  $\varepsilon_{\text{cmb}} = 6.3 \times 10^{-4} \text{ eV}$ , which provides IC scattering, and higher energy  $\tilde{\varepsilon}_{\text{cmb}}$ , which provides absorption of cascade photons with minimum energy  $\tilde{\mathcal{E}}_{\text{min}}$  given by Eq. (18). As physics is concerned

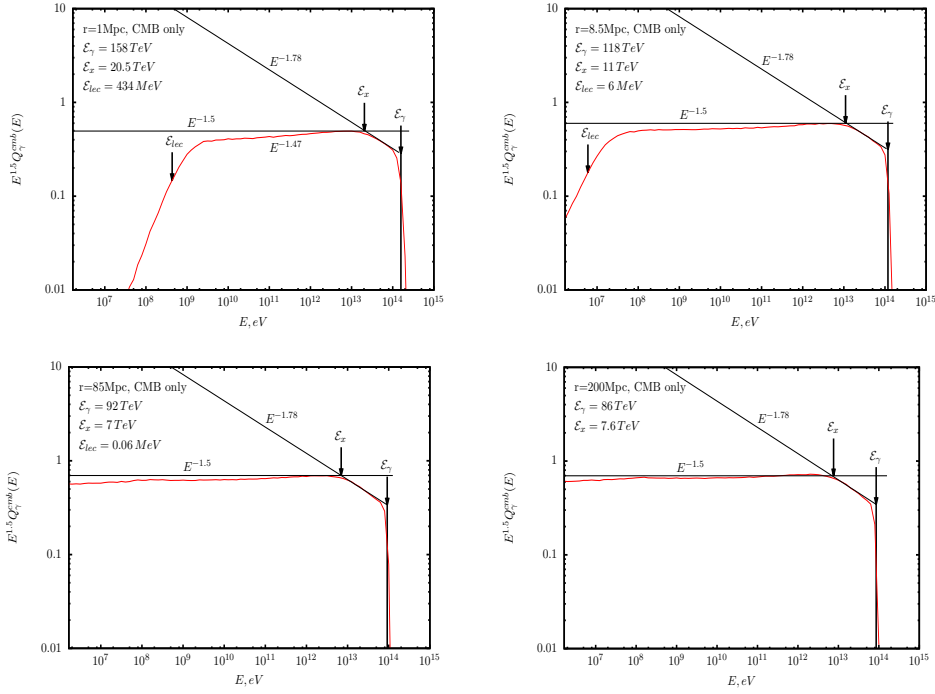


FIG. 6: Comparison of analytic calculations with numerical simulations for CMB radiation only for nearby sources at distances 1.0 Mpc, 8.5 Mpc, 85 Mpc and 200 Mpc.

$\tilde{\varepsilon}_{\text{cmb}}$  is minimal energy in HE Planckian tail of photon distribution where number density of photons is big enough enough for absorption of photons with energy  $\tilde{\varepsilon}_{\text{min}}$ . The energy  $\varepsilon_{\text{min}}$  for  $\tilde{\varepsilon}_{\text{min}}$  can be calculated from kinematic relation for arbitrary  $E_\gamma$  and  $\varepsilon$  given by  $E_\gamma \varepsilon (1 + \cos \phi) = 2\varepsilon_{\text{cm}}^2$ , where  $\phi$  is an angle between photons  $E_\gamma$  and  $\varepsilon$  in laboratory system and  $\varepsilon_{\text{cm}}$  is energy of each photon in cm-system. Finding the value  $\varepsilon$  from this relation for  $E_\gamma = \tilde{\varepsilon}_{\text{min}}$  and minimizing it with the choice  $\cos \phi = 1$  and  $\varepsilon_{\text{cm}} = m_e$ , we arrive at  $\varepsilon_{\text{min}} = m_e^2 / \tilde{\varepsilon}_{\text{min}}$  as in Eq. (18).

We can discuss now the spectra and basic features predicted for the cascades on CMB from nearby sources, assuming tentatively, as the first step,  $\varepsilon_{\text{cmb}} \sim 6 \times 10^{-4}$  eV and  $\tilde{\varepsilon}_{\text{cmb}} \sim 2 \times 10^{-3}$  eV (these values will be determined more precisely after comparison with numerical simulations.)

The minimum absorption energy (on CMB photons) can be estimated from equation  $\ell_{\text{abs}}^{\text{cmb}}(\tilde{\varepsilon}_{\text{min}}) = r$ , where  $\ell_{\text{abs}}^{\text{cmb}}(E_\gamma)$  is absorption length in CMB background. It results in well known value  $\tilde{\varepsilon}_{\text{min}} \sim 1 \times 10^{14}$  eV and it is given precisely, as  $\tilde{\varepsilon}_\gamma$ , for different distances  $r$  in Table I. Using Eq. (18) we find then  $\tilde{\varepsilon}_{\text{cmb}} \sim 2 \times 10^{-3}$  eV. The transition energy is given by  $\mathcal{E}_X = (1/3)(\tilde{\varepsilon}_{\text{min}}/m_e)^2 \varepsilon_{\text{cmb}}$  which approximately equals to  $7 \times 10^{12}$  eV. We cannot expect in this picture the standard spectra  $\propto E^{-1.5}$  and  $\propto E^{-2}$ , especially the latter one. First of all the spectrum can be flatter than  $\propto E^{-2}$  due to flattening of  $E_\gamma \propto E_e^{-2}$  regime in the end of the IC spectrum (see Fig. 2).

Another plausible reason is the width of the cascade-multiplication part of the spectrum, i.e. one with conventional  $E^{-2}$  spectrum, but with ratio  $\mathcal{E}_\gamma/\mathcal{E}_X \approx 14$  to be compared with  $3 \times 10^3$  for the case of  $(\varepsilon_{\text{cmb}}, \varepsilon_{\text{ebl}})$  background. The relatively small ratio  $\mathcal{E}_\gamma/\mathcal{E}_X \approx 14$  is the reminiscent of the ratio 3 for CMB monochromatic background model (see Eq. (14)). Since the realistic simulations show a smooth transition between energies  $\mathcal{E}_X$  and  $\mathcal{E}_\gamma$ , one may expect non-power-law of cascade-multiplication spectrum, in disagreement with the dichromatic model. As for low-energy asymptotic spectrum  $E^{-1.5}$ , it also should be distorted, because absorption on  $\tilde{\varepsilon}_{\text{cmb}}$  photons occurs at distances of order of distance to the source  $r$  and thus a cascade is underdeveloped. Now we will compare the analytic estimates with accurate numerical simulations for cascades on CMB radiation, and obtain more precisely parameters of our dichromatic model for different distances  $r$  to the source. We will change the notation as  $\tilde{\varepsilon}_{\text{min}} \equiv \tilde{\varepsilon}_\gamma$  to emphasize that this is the value of spectrum cutoff.

As the first step we find  $\tilde{\varepsilon}_\gamma$  from equation  $\ell_{\text{abs}}^{\text{cmb}}(\tilde{\varepsilon}_\gamma) = r$ , where  $\ell_{\text{abs}}^{\text{cmb}}(E_\gamma)$  is absorption length in CMB background. The values of  $\tilde{\varepsilon}_\gamma$  are shown in Table I for distances 1.0 , 8.5 , 85 , and 200 Mpc.

Next we calculate  $\tilde{\varepsilon}_{\text{cmb}}$  using Eq. (18) and values of  $\tilde{\varepsilon}_{\text{min}} \equiv \tilde{\varepsilon}_\gamma$  from the Table I (third row).

The values of  $\mathcal{E}_X$  in the fourth row are obtained from comparison with numerical simulations (see Fig. 6) as in-

tersection of the power-law approximation of the cascade-multiplication spectrum ( $\propto E^{-1.8}$  in the Fig. 6) with low-energy asymptotic.

The energies of CMB photons  $\varepsilon_{\text{cmb}}$  (fifth row) are calculated using the equation  $\mathcal{E}_X = (1/3)(\mathcal{E}_\gamma/m_e)^2 \varepsilon_{\text{cmb}}$ .

In the last row of Table I we put the low-energy cutoff  $\mathcal{E}_{\text{lec}}^\gamma$  of the cascade spectrum estimated in the following way.

The low-energy cascade electrons with energy below some critical energy  $E_e^{\text{cr}}(r)$  have a time of IC photon emission larger than time-of-flight  $r/c$ . Therefore radiation of IC photons with energies below  $\mathcal{E}_{\text{lec}}^\gamma = (4/3)(E_e^{\text{cr}}/m_e)^2 \varepsilon_{\text{cmb}}$  is suppressed.

The critical energy of electron  $E_e^{\text{cr}}$  can be found from  $\tau_e^{-1}(E_e^{\text{cr}}) = c/r$ , where  $\tau_e(E)$  is the electron lifetime relative to IC energy loss:

$$\tau_e^{-1}(E_e) = \left( \frac{1}{E_e} \frac{dE_e}{dt} \right)_{\text{IC}} = \frac{4}{3} \sigma_T c \gamma_e \frac{\rho_{\text{cmb}}}{m_e}, \quad (19)$$

where  $\sigma_T$  is the Thompson cross-section,  $\gamma_e = E_e/m_e$  is the electron Lorentz-factor and  $\rho_{\text{cmb}} = \varepsilon_{\text{cmb}} n_{\text{cmb}}$  is energy density of CMB radiation. Eq. (19) can be rearranged as

$$\tau_e^{-1}(E_e) = \frac{4}{3} \sigma_T c n_{\text{cmb}} \frac{E_e}{\mathcal{E}_\gamma} \quad (20)$$

where  $\mathcal{E}_\gamma^{\text{cmb}} = m_e^2 / \varepsilon_{\text{cmb}}$ .

Using  $\tau_e^{-1}(E_e^{\text{cr}}) = c/r$  one finds the critical energy of electron  $E_e^{\text{cr}}$  and low-energy cutoff  $\mathcal{E}_{\text{lec}}^\gamma$  as

$$E_e^{\text{cr}} = \frac{3/4}{\sigma_T n_{\text{cmb}} r} \mathcal{E}_\gamma^{\text{cmb}}, \quad \mathcal{E}_{\text{lec}}^\gamma = \frac{3}{4} \left( \frac{1}{\sigma_T n_{\text{cmb}} r} \right)^2 \mathcal{E}_\gamma^{\text{cmb}} \quad (21)$$

From Table I one can see that for nearby sources at distance 1 - 85 Mpc the dichromatic model is characterized by almost equal energies  $\varepsilon_{\text{cmb}} \approx 6 \times 10^{-4}$  eV and by similar values of  $\tilde{\varepsilon}_{\text{cmb}} \approx (2-3) \times 10^{-3}$  eV. For 200 Mpc these values differ more considerably. The low-energy cutoff is observable only for very close sources  $\mathcal{E}_{\text{lec}}^\gamma \sim 400$  MeV for  $r = 1$  Mpc; for  $r = 8.5$  Mpc it starts at 6 MeV.

Finally we calculate the cascade-photon spectrum taking the characteristic energy features from Table I and compare this spectrum with precise numerical simulation on CMB radiation only. One may expect that canonical low-energy part of spectrum  $\propto E^{-1.5}$  will survive for long-distance sources and may fail for short-distance ones, being underdeveloped. The Fig. 6 confirms this expectation: for distance  $r = 200$  Mpc the spectrum coincides well with  $E^{-1.5}$  shape, and weakly distorted at smaller distances. For high-energy part of the spectrum ( $\mathcal{E}_X - \mathcal{E}_\gamma$ ) the energy interval is very short and spectrum is  $\propto E^{-1.78}$  flatter than canonical 2.0 .



TABLE I: Parameters of analytic model for nearby sources (CMB only).

distance $r$	1 Mpc	8.5 Mpc	85 Mpc	200 Mpc
$\bar{\mathcal{E}}_\gamma$ eV	$1.58 \times 10^{14}$	$1.18 \times 10^{14}$	$9.24 \times 10^{13}$	$8.6 \times 10^{13}$
$\bar{\mathcal{E}}_{\text{cmb}}$ eV	$1.65 \times 10^{-3}$	$2.21 \times 10^{-3}$	$2.83 \times 10^{-3}$	$3.04 \times 10^{-3}$
$\mathcal{E}_X$ eV	$2.05 \times 10^{13}$	$1.11 \times 10^{13}$	$7.0 \times 10^{12}$	$7.6 \times 10^{12}$
$\varepsilon_{\text{cmb}}$ eV	$6.42 \times 10^{-4}$	$6.24 \times 10^{-4}$	$6.43 \times 10^{-4}$	$8.0 \times 10^{-4}$
$\mathcal{E}_{\text{lec}}^\gamma$ eV	$4.34 \times 10^8$	$6.01 \times 10^6$	$6.01 \times 10^4$	$1.09 \times 10^4$

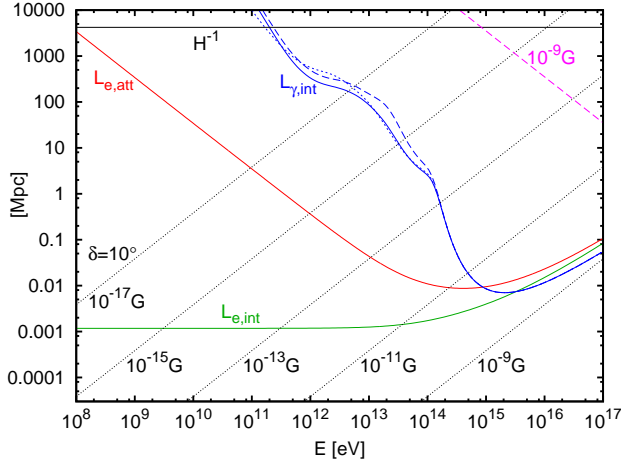


FIG. 7: Shown are: pair production interaction length (see Eq. 22) calculated assuming EBL models of Ref. [16] (shown by solid blue line), of Ref. [17] (dashed blue line) and of Ref. [37] (dotted blue line); electron attenuation length (see Eq. 23) due to inverse Compton scattering (red line) and interaction length of this process (green line);  $10^\circ$  deflection length for electrons (shown by black dotted lines) for given values of constant transverse component of magnetic field; synchrotron energy loss length (see Eq. 28) of electrons in  $B_\perp = 10^{-9}\text{G}$  (shown by pink dashed line); adiabatic energy loss length (shown by horizontal solid black line).

### III. NUMERICAL SIMULATIONS OF ELECTROMAGNETIC CASCADE PROPAGATION

In this section we will discuss the basics of numerical simulations, universality of em-cascade spectra in the numerical simulations, the calculated cascade energy spectra and upper limits on cascade energy density  $\omega_{\text{cas}}$  obtained from comparison of the calculated spectra with observations of Fermi LAT.

#### A. Generalities

The results presented in this work have been obtained with two independent numerical techniques, the Monte Carlo simulation and the code [38, 39] based on solution of Boltzmann kinetic equations for cascade particles propagation in one dimension. The latter method doesn't take into account deflections of cascade particles by magnetic field and therefore is valid only for calculations with averaged angles and time or for diffuse fluxes. In Fig. 7 interaction and energy loss lengths are shown for electrons and photons. The lengths are defined as follows:

$$L_{i,\text{int}}^{-1} = \int d\epsilon n(\epsilon) \int d\mu \frac{1 - \beta_i \mu}{2} \sigma_i \quad (22)$$

$$L_{e,\text{att}} = L_{e,\text{int}} E_e / \bar{E}_\gamma, \quad (23)$$

where  $i = e, \gamma$ ;  $\sigma_e = \sigma_{IC}$ ;  $\sigma_\gamma = \sigma_{\text{PP}}$  and  $\bar{E}_\gamma$  is the mean energy of the recoil photon in IC. A number of kinetic equation-based codes has been developed at present (see e.g. [38, 40, 41]). For precise calculation of  $\gamma$ -ray fluxes from individual sources in presence of non-negligible magnetic fields, full 3D Monte Carlo simulation is needed. Such calculations as a rule require excessive computing time since number of secondary particles grows exponentially in the cascade. In the Monte Carlo code used in this work to speed up computations we utilize, following Ref. [35], the weighted sampling of the cascade development. It allows us reduce the number of secondary particles.

While IC scattering occurs mostly on CMB, the  $e^+e^-$  pair production, when it is below threshold on CMB, takes place on infra-red and optical components of EBL which is not precisely known. A number of different models have been proposed for EBL [16, 17, 37, 42–45]. There are some upper bounds on EBL in the literature that were based on observations of distant blazars. These limits are derived without taking into account the contribution of cosmic rays and therefore these bounds can be relaxed [46], and only limits based on GRBs [47] remain unaffected. The model of Ref. [44] is disfavoured by Fermi LAT observation of the photons from GRB 090902B and GRB 080916C. To obtain the range of  $\omega_{\text{cas}}$  in this work we use the baseline model from the recent work [37] which includes estimates of EBL for redshifts  $z \leq 10$ . In addition we use for comparison the "best fit" and "lower-limit" models of Refs. [16, 17], providing estimates of EBL for  $z \leq 5$ . The EBL model of Ref. [43] for  $z \leq 2$  is used only for comparison of our numerical calculations with work [29].

Another poorly known factor which is crucial for consideration of the electromagnetic cascades from individual sources is intergalactic magnetic field (IGMF). Even in presence of relatively weak IGMF the angular size of sources can increase due to deflection of electrons and positrons moving along the curved trajectories with cur-

vature radius  $R_c$

$$R_c = \frac{E_e}{eB} \simeq 1.1 \left( \frac{E_e}{1 \text{ TeV}} \right) \left( \frac{B_\perp}{10^{-15} \text{ G}} \right)^{-1} \text{ Mpc}. \quad (24)$$

After traversing distance  $L$  the misalignment of the electron direction with the primary  $\gamma$ -ray direction is given by angle  $\delta$ :

$$\delta \simeq \begin{cases} \frac{L}{R_c}, & L \ll \lambda_B \\ \frac{\sqrt{L\lambda_B}}{R_c}, & L \gg \lambda_B. \end{cases} \quad (25)$$

where  $\lambda_B$  is IGMF correlation length. In the second case above, many stochastic deflections were taken into account. The deflections in the cascade can not be neglected as soon as electron energy-loss length becomes comparable with defocusing length i.e. the travel path at which electrons are deflected by maximal angle  $\delta$ . The definition of  $\delta$  varies for different problems. It may be related to experimental angular resolution or average angular distance between the sources. The defocusing lengths for  $\delta = 10^\circ$  and a range of IGMF strengths (assuming  $\lambda_B \gg L$ ) are shown in Fig. 7 (black dashed lines) together with the energy-loss length (red curve) for comparison. As example in case  $B = 10^{-15} \text{ G}$  and  $\delta = 10^\circ$  one can infer that deflections become important for electron energy  $E_e \lesssim 1 \text{ TeV}$  which corresponds to typical recoil photon energy of  $3 \text{ GeV}$ . Below this energy  $\gamma$ -ray flux is essentially isotropized.

Current theoretical and observational constraints on the IGMF mean value and correlation length are summarized in the review [22] as

$$10^{-17} \text{ G} \lesssim B \lesssim 10^{-9} \text{ G}, \quad (26)$$

$$\lambda_B \gtrsim 1 \text{ pc}; \quad (27)$$

where the obtained lower limit on IGMF is based on the simultaneous observation of GeV and TeV gamma-radiation from the hard-spectrum blazars RGB J0710+591, 1ES 0229+200, and 1ES 1218+304 (Fermi/LAT-observations in GeV, and Veritas, MAGIC and HESS observations in TeV) [29].

In the special case of IGMF being close to it's upper limit  $B \simeq 10^{-9}$  and for the sources emitting ultra-high energy photons or electrons with  $E \gtrsim 10^{19} \text{ eV}$ , the electron synchrotron losses should be taken into account. Pink line on Fig. 7 represents energy loss-length for this process given by [48].

$$L_{syn}^{-1} = \frac{1}{E_e} \frac{dE_e}{dt} = -\frac{4}{3} \sigma_T \frac{B^2}{8\pi} \frac{E_e}{m_e^2} \quad (28)$$

where  $\sigma_T$  is the Thomson cross section, and  $m_e$  is the electron mass. In this paper we disregard the synchrotron energy losses if not otherwise stated.

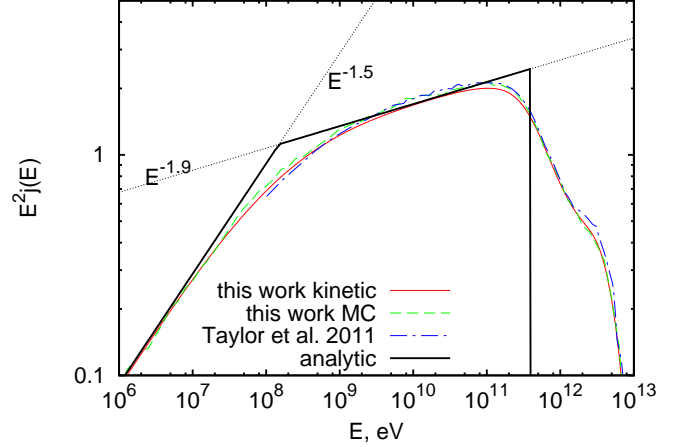


FIG. 8: Average cascade spectrum obtained using kinetic equation code (solid curve) and Monte Carlo code (dashed curve) compared with analytic calculation and with results of Monte Carlo simulation [29] (dot-dashed curve), all for injection of  $10^{14} \text{ eV}$  photons at  $z = 0.13$ .

## B. Comparison

In this section we compare the cascade spectra obtained using the kinetic equation and Monte Carlo codes from the present work with other numerical simulations and with analytic calculations. Fig. 8 demonstrates level of agreement between our numerical calculations, simulation [29], and analytic calculation for a source at  $z = 0.13$  injecting  $10^{14} \text{ eV}$  photons and using EBL model of Ref. [43] for photon absorption. One may see in this figure the familiar two cascade energy spectra  $\propto E^{-1.5}$  and  $\propto E^{-1.9}$  and also the steeper high energy feature in a good agreement in all three numerical simulations. As will be demonstrated below this feature plays an important role in determination of the cascade energy density  $\omega_{cas}$ .

The diffuse gamma-ray spectrum as presented by Fermi LAT in 2015 [7] shows the steepening which starts at  $1 \times 10^{11} \text{ eV}$  and continues as more sharp cutoff at  $\epsilon = 2.5 \times 10^{11} \text{ eV}$ . The both high energy features in theoretical spectra in Fig. 8,  $\propto E^{-1.9}$  and more steep feature above it, are more flat than that observed by Fermi LAT and it results in the upper limit on  $\omega_{cas}$ . The reason may be easily understood from Fig. 8.

For given large enough  $\omega_{cas}$  the realistic, numerically calculated, spectra from Fig. 8 can intersect the Fermi high energy tail at some energy. It means that at energy above the crossing the calculated cascade flux is larger than the measured Fermi flux. To eliminate this contradiction one must lower the calculated cascade flux, i.e.  $\omega_{cas}$ . This procedure results in the upper limit on  $\omega_{cas}$ .

The case of analytic spectrum in Fig. 8 is quite different. It has a sharp cutoff at  $\epsilon_\gamma \approx 400 \text{ GeV}$  close to Fermi

cutoff energy  $\epsilon \approx 250$  GeV and thus quite larger  $\omega_{\text{cas}}$  is allowed.

All effects which make lower the high-energy cutoff in the calculated cascade spectrum, e.g. high red-shift of production, *increase* the upper limit on  $\omega_{\text{max}}$ .

#### IV. UNIVERSALITY OF THE CASCADE SPECTRA IN NUMERICAL SIMULATIONS

Universality of the cascade energy spectrum was discovered first in analytic calculations [34], and we will start our discussion from analytic dichromatic model of section II A. This universality is clearly seen from Eq. (9), where two joint energy spectra  $\propto E^{-3/2}$  and  $\propto E^{-2}$  appear, divided by two boundary energies  $\mathcal{E}_X$  and  $\mathcal{E}_\gamma$ , built from basic parameters of dichromatic model  $\varepsilon_{\text{cmb}}$  and  $\varepsilon_{\text{ebl}}$ . The main features of this universal spectrum include: (i) The same energy shape of the spectrum produced by initial photon/electron if its primary energy is sufficiently high. Ultimately the scale can be as high as  $E_0 \gtrsim m_e^2/\varepsilon_{\text{cmb}} \sim 0.4$  PeV and it is the basic one in analytic calculations. The lower universality scale  $E_0 \sim 100$  TeV is found in numerical simulations and this result is very natural and may be expected apriori. In analytic approach the cutoff energy  $\mathcal{E}_\gamma^{\text{cmb}} = 0.4$  PeV is consequence of monochromatic spectrum of CMB photons  $\epsilon_{\text{cmb}} = 6.3 \times 10^{-4}$  eV. In numerical simulations absorption occurs on high-energy tail of Planckian distribution of CMB photons and absorption produced at  $\mathcal{E}_\gamma^{\text{cmb}} \approx 100$  TeV when  $\ell_{\text{abs}}$  reaches  $c/H_0$ . (ii) The cascade energy spectrum is the same for any injection spectrum  $Q(E_s)$  at  $E_s \gtrsim E_0$  (in other words cascade spectrum forgets what injection spectrum produced it). (iii) The cascade spectrum does not depend on distance to the point where cascade started, and (iv) Energy density of the cascade  $\omega_{\text{cas}}$  is the only cascade characteristic which determines the spectrum.

These properties of 'analytic' cascades will be referred to as *strong universality*.

For realistic cascades in the expanding universe the strong universality, as it is formulated above, is not valid. The cascade spectrum observed at  $z = 0$  depends on redshift of production  $z_s$ , e.g. due to dependence  $\mathcal{E}_X$  and  $\mathcal{E}_\gamma$  on  $z_s$  and simply due to redshift of the spectrum. Consider for example the generation rate of photons/electrons in expanding universe in the form  $Q(E_s, z_s) = \phi(E_s)R(z_s)$  with  $E_s$  above the universality scale  $E_0$ . All cascades produced at fixed redshift  $z_s$  have the same cascade spectrum  $q_{\text{cas}}(E)$  at  $z = 0$ . However, cascades originated at different  $z_s$  have the different cascade spectra at  $z = 0$ , and integration over  $z_s$  results in cascade spectra, which depend on distribution of production rate  $Q(E_s, z_s)$  over  $z_s$ . Predicted cascade spectrum is determined not only by  $\omega_{\text{cas}}$  but e.g. by parameters of cosmological evolution of the sources. Universality of the cascade spectra remains only for a subclass of the sources with approximately equal redshifts. In summary, the

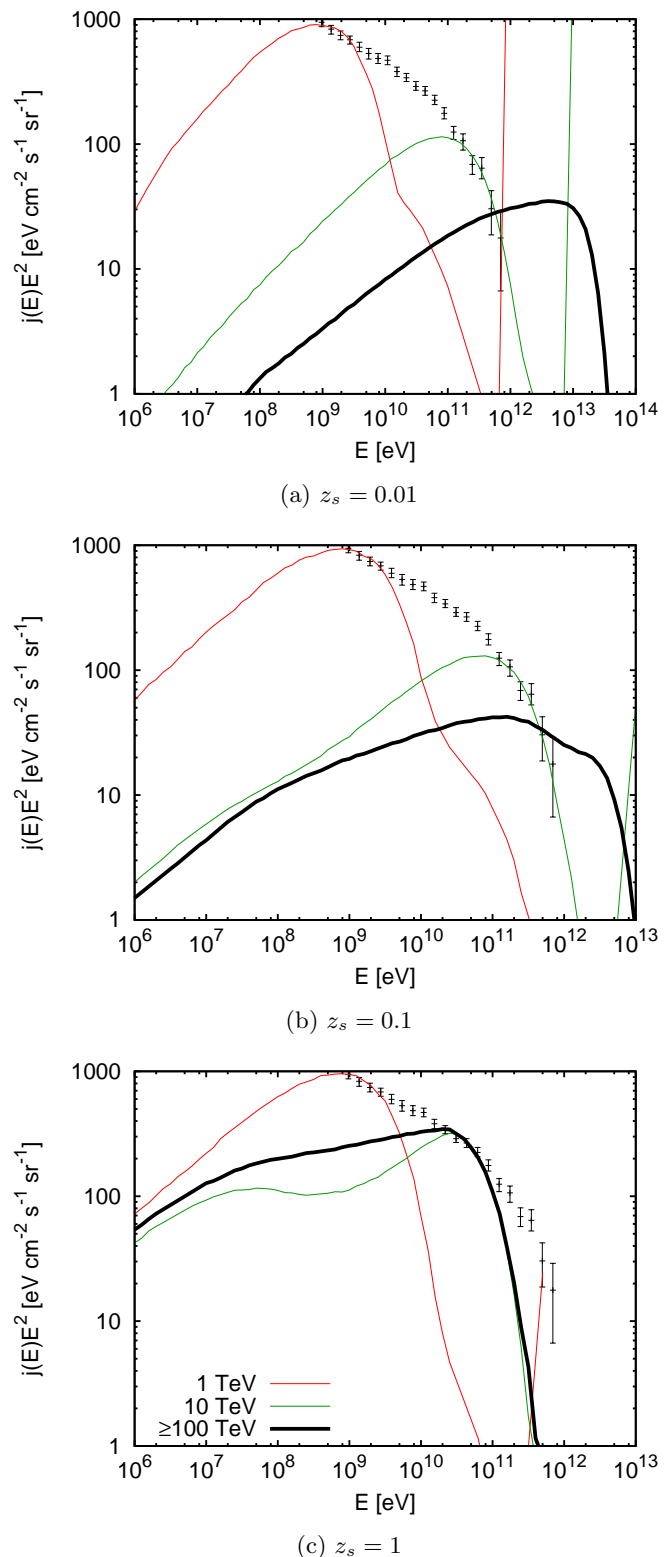


FIG. 9: Diffuse cascade spectrum from sources injecting photons with energy  $E_s = 1$  TeV (red curves), 10 TeV (green curves) and  $E_s \geq 100$  TeV (black thick curves) at redshifts  $z = 0.01$ ,  $z = 0.1$ ,  $z = 1$ . Photon fluxes are limited from above by the Fermi EGB flux, shown by black errorbars, with foreground model B [7]. The curves obtained for initial photon energies greater than 100 TeV coincide in all figures. In calculations the EBL flux from Ref. [37] is used.

sources in expanding universe with the generation rate  $Q(E_s, z)$ , with  $E_s$  above the universality scale  $E_0$  and with arbitrary dependence on  $z$  (e.g. evolution  $(1+z)^m$  up to  $z_{\max}$ ) have the following properties of universality: (i) energy shape of em-cascade at  $z = 0$  is independent from  $E_s$  or from injection spectrum  $\phi(E_s)$ , i.e. for fixed  $z_s$  the shape is the same for different  $E_s$ , or for different spectra  $\phi(E_s)$ , (ii) cascade spectrum at  $z = 0$  is not uniquely determined by  $\omega_{\text{cas}}$ , but depends also on evolution of  $Q(E, z)$  with  $z$ , e.g. through parameters  $m$  and  $z_{\max}$ , (iii) a subclass of the sources with the same (or almost the same) redshift  $z_s$  has the identical cascade spectrum at  $z = 0$ , which is characterized by the single parameter  $\omega_{\text{cas}}$ .

This case can be referred to as *weak universality*.

Class of sources with the fixed redshift of production  $z_s$ , i.e with production rate  $Q(E_s, z) = \phi(E_s)\delta(z-z_s)$  has all properties of strong universality, except (iii), and can be attributed to *strong universality* for arbitrary generation spectrum  $\phi(E_s)$  with  $E_s$  above the universal scale  $E_0$ . The corresponding cascade spectrum is characterized by a single parameter  $\omega_{\text{cas}}$  for any fixed  $z_s$ .

Consider  $z$ -fixed sources in some details, starting from low initial energy  $E_s < E_0$ . At increasing  $E_s$  the  $z = 0$  cascade spectrum must evolve to strongly-universal spectrum and reaching it at scale  $E_0$  stay unchanged. Fig. 9 illustrates this statement. The figure presents the diffuse fluxes generated by the population of sources with the fixed energy of injected photon  $E_s$  and with fixed redshift  $z_s$ . The diffuse spectrum *shape* at  $z = 0$  doesn't depend on  $E_s$  as long as  $E_s \gtrsim \mathcal{E}_\gamma^{\text{cmb}}$ . In fact, for remote enough sources at  $z \gtrsim 0.1$ , universality is reached at the scale  $E_0 \gtrsim 100$  TeV. This observation was tested for all EBL models used in this work.

The numerically calculated diffuse cascade spectra from the sources with fixed redshift  $z_s$  and energy  $E_s$  are shown in Figs 9a - 9c. The spectra are expected to be strongly universal when energy  $E_s$  exceeds the largest scale  $E_0 = \mathcal{E}_\gamma^{\text{cmb}} = 0.4$  PeV. All three figures (a), (b) and (c) demonstrate that the spectra are universal at  $E \geq E_0$ , where  $E_0 = 100$  TeV. This energy can be considered as energy scale of universality in numerical simulations (see discussion above). Apart from identical spectra they have at large  $z_s \geq 0.1$  the predicted standard spectrum  $\propto E^{-3/2}$  at low energy,  $\propto E^{-1.9}$ , at intermediate energies with highest energy feature in the end of the spectrum (cf with Fig. 8). The spectra with  $E_s = 100$  TeV (black thick curves) and with all energies  $E_s \gtrsim 100$  TeV are indistinguishable in Figs 9.

The cascade universality makes it hard to extract the injection spectrum from the diffuse spectrum observed at  $z = 0$ . On the other hand the comparison of the calculated and observed spectra allows us to estimate the upper limit on the main characteristic of the universal cascade spectrum, the cascade energy density  $\omega_{\text{cas}}$  at  $z = 0$ . This problem will be considered in the next section.

## V. UPPER LIMIT ON $\omega_{\text{cas}}$ FROM FERMI LAT DATA

The upper limit on the cascade energy density given by Eq. (1) as  $5.8 \times 10^{-7}$  eV/cm<sup>3</sup> has been derived in [36] from the first-year Fermi data [6]. Here we obtain this limit from 50 months Fermi LAT observations [7] using somewhat different approach.

Fermi LAT [6] presents two kinds of extragalactic gamma-ray fluxes in energy range 100 MeV - 820 GeV: EGB (Extragalactic  $\gamma$ -ray Background) and IGRB (Isotropic diffuse  $\gamma$ -ray Background), EGB presents the total extragalactic gamma-ray flux, from which about half is given by the resolved individual sources. In the cascade calculations we use these fluxes to normalize the upper limits on the cascade energy density  $\omega_{\text{cas}}$ . The highest and most conservative upper limit on theoretical energy density  $\omega_{\text{cas}}$  is imposed by Fermi EGB flux and is marked as  $\omega_{\text{cas}}^{\text{tot}}$ . In isotropic case the estimate of  $\omega_{\text{cas}}^{\text{iso}}$  can be obtained from Fermi IGRB flux [7] assuming additionally highly homogeneous distribution of gamma-ray sources or astrophysical  $\gamma$ -ray generation scenarios where Intergalactic Magnetic Field (IGMF) must be high enough to isotropise the cascade electrons and positrons (or their parent particles) in the space.

EGB flux is higher than IGRB, and the two calculated values of  $\omega_{\text{cas}}$  follow this hierarchy. Both fluxes are described by power-law spectrum with index  $\gamma \approx 2.3$  and with more steep highest energy tail starting at  $E_{\text{cut}} = \epsilon \approx 250$  GeV (beginning of the steepening). The nature of gamma-ray flux above  $E_{\text{cut}}$  is not well known, but we consider it as diffuse flux. This high-energy steep component (tail) is responsible for stronger upper limit on  $\omega_{\text{cas}}$  in comparison with earlier paper [8]. The realistic, numerically calculated, spectra in Fig. 8 are flatter than the highest-energy Fermi tail and can intersect it at some energy (see section III B).

### A. Upper limit on $\omega_{\text{cas}}$ in analytic calculations

To illustrate our method of calculating  $\omega_{\text{cas}}$  we will consider first a simple example of analytic model followed then by the accurate numerical calculations.

Consider the energy of Fermi IGRB spectrum cut-off  $\epsilon = 2.5 \times 10^5$  MeV, where the measured flux is  $J_\gamma^{\text{igrb}} = 4.80 \times 10^{-16} \text{cm}^{-2} \text{s}^{-1} \text{sr}^{-1} \text{MeV}^{-1}$ . We use here the analytic dichromatic model with  $\epsilon_{\text{cmb}} = 6.3 \times 10^{-4}$  eV and  $\epsilon_{\text{ebl}} \approx 1$  eV, which provides the high-energy cutoff in the cascade spectrum  $\mathcal{E}_\gamma = m_e^2/\epsilon_{\text{ebl}} = 2.61 \times 10^5$  MeV, practically the same as observed in Fermi IGRB spectrum  $\epsilon = E_{\text{cut}}$ . We take the cascade spectrum as  $J_{\text{cas}}(E) \propto E^{-1.9}$  at  $\mathcal{E}_X \leq E \leq \mathcal{E}_\gamma$  and  $E \propto E^{-1.5}$  at  $E \leq \mathcal{E}_X$ . Then the cascade energy density can be calcu-



lated using the cascade flux  $J_{\text{cas}}(E)$  as

$$\omega_{\text{cas}} = \frac{4\pi}{c} \left( \int_0^{\mathcal{E}_X} dE E J_{\text{cas}}(E) + \int_{\mathcal{E}_X}^{\mathcal{E}_\gamma} dE E J_{\text{cas}}(E) \right) \quad (29)$$

The most restrictive relation we use in calculation of Eq. (29) is given by the cascade flux in energy interval  $\mathcal{E}_X \leq E \leq \mathcal{E}_\gamma$

$$J_{\text{cas}}(E) = J_{\text{igrb}}(\epsilon)(E/\epsilon)^{-1.9}, \quad (30)$$

which includes normalization of the cascade flux by Fermi IGRB flux  $J_{\text{igrb}}$  at energy  $\epsilon = E_{\text{cut}}$ . This particular condition provides the low upper limit on  $\omega_{\text{cas}}$  in this estimate.

For interval  $E \leq \mathcal{E}_X$  we use

$$J_{\text{cas}}(E) = J_{\text{igrb}}(\epsilon)(\mathcal{E}_X/\epsilon)^{-1.9}(E/\mathcal{E}_X)^{-1.5} \quad (31)$$

As a result we obtain the upper limit on energy density of cascade radiation

$$\omega_{\text{cas}} \leq 6.6 \frac{4\pi}{c} \epsilon^2 J_{\text{igrb}}(\epsilon) = 8.3 \times 10^{-8} \text{ eV/cm}^3, \quad (32)$$

to be compared with much larger cascade upper limit  $\omega_{\text{cas}}^{\text{max}} = 5.8 \times 10^{-7} \text{ eV/cm}^3$  obtained in [8] and used in [9]. The reason is that for normalization of calculated flux we used the measured flux at energy  $\epsilon = 2.5 \times 10^5 \text{ MeV}$ , which is located below the Fermi  $E^{-2.3}$  approximation of the flux. However, this argument implies the further decrease of  $\omega_{\text{cas}}^{\text{max}}$ . In more realistic numerical simulations there is the high-energy tail (see Fig. 8) and intersection of this tail with steep high-energy Fermi IGRB tail demands lowering the calculated flux, i.e. further suppression of  $\omega_{\text{cas}}$ . Another reason of modification of calculated spectrum is connected with interpretation of two highest energy points in the Fermi LAT spectrum above  $2.5 \times 10^5 \text{ MeV}$ . If these points belong to isotropic diffuse radiation the high-energy theoretical tail must be shifted downward and it results in lowering of  $\omega_{\text{cas}}$ . However, in case the weak universality  $\omega_{\text{cas}}$  is not the only parameter which influence the flux, it could be that other parameters, e.g. the cosmological evolution of the sources, can shift the flux upward at the same  $\omega_{\text{cas}}$ .

The stronger upper limit on  $\omega_{\text{cas}}^{\text{iso}}$  obtained here put the stronger upper limit on the flux of UHE extragalactic protons and cosmogenic neutrinos, in comparison with [8–10]. The effect of increasing the fraction of resolved sources [52] diminishes further  $J_{\text{cas}}(E)$  and  $\omega_{\text{cas}}$  given above.

## B. Upper limit on $\omega_{\text{cas}}$ in numerical simulations

Now we will proceed to consideration of  $\omega_{\text{cas}}$  using the calculation of the cascade spectra in numerical simulations, kinetic equations and Monte Carlo. These calculations provide us with the shape of the cascade spectra at

$E < \epsilon_\gamma$ , and normalization by the observed Fermi LAT spectrum allows us to obtain the values of  $\omega_{\text{cas}}$ , the final aim of our research in this paper.

Below we calculate  $\omega_{\text{cas}}^{\text{tot}}$  and  $\omega_{\text{cas}}^{\text{iso}}$  for two cases: (i) the redshift-fixed photon-electron sources with very high energy  $E_s$  and (ii) redshift-distributed sources with injection rate of photons/electrons  $Q(E_s, z)$  smoothly dependent on  $z$ . The case (i) results in strong universality and (ii) for general case of  $z$  dependence, in weak universality. The scale of very high energy is given by  $E_s \gtrsim \mathcal{E}_\gamma^{\text{cmb}} \gtrsim 0.4 \text{ PeV}$  for analytic calculations, though as argued above and as Figs 9a - 9c show, the universal shape of the spectra is reached already at energy scale  $E_s \sim 100 \text{ TeV}$ .

Let us now come over to numerical calculation of the cascade spectra and to evaluation of  $\omega_{\text{cas}}$ . We consider two cases:

(i) The redshift-fixed and energy-fixed sources with injection rate

$$Q(E, z) \propto \delta(z - z_s) \delta(E - E_s), \quad (33)$$

and

(ii) Redshift-distributed sources with injection rate

$$Q(E, z) = (1 + z)^{3+m} \delta(E - E_s), \text{ at } z < z_{\text{max}}, \quad (34)$$

with  $1 < z_{\text{max}} < 5$  and  $0 < m < 5$  (the case  $m = 0$  corresponds to constant source density in comoving frame).

In calculations for both cases we will keep  $E_s \geq 100 \text{ TeV}$  to provide universality.

The calculated spectra will be normalized by Fermi LAT spectra, EGB and IGRB. The highest and most conservative upper limit on energy density  $\omega_{\text{cas}}$  is imposed directly by EGB flux, which includes also the flux of resolved extragalactic discrete sources. To be even more conservative we take the fluxes of EGB (and IGRB too) as maximal one allowed by systematic uncertainties. Using these two fluxes we obtain the upper limits on  $\omega_{\text{cas}}^{\text{igrb}}$  and  $\omega_{\text{cas}}^{\text{egb}}$ , the latter will be considered as maximally allowed  $\omega_{\text{max}}$ .

In case (i) the spectra are shown for three values of  $z_s$  in Figs. 9a - 9c. At energies  $E_s$  higher than 100 TeV all spectra are the same. Fig. 10 presents the cascade spectra for continuous source distribution (34), which illustrates the dependence of the cascade spectra on evolution parameters  $m$  and  $z_{\text{max}}$ .

From Fig. 10 one may observe that spectra with low  $z_{\text{max}} = 1$  have large cutoff-energy  $E_{\text{max}}$  and to avoid the contradiction with Fermi data one must shift the calculated spectrum downwards, diminishing thus  $\omega_{\text{cas}}$ .

Spectra with large  $z_{\text{max}} = 5$  have lower  $E_{\text{max}}$  due to redshift factor  $(1 + z)$  and respectively larger  $\omega_{\text{cas}}$ . Dependence on  $m$  works in the similar way. Fig. 10 allows us to calculate  $\omega_{\text{cas}}$  using the corresponding curves. As a result the constraints on energy density of cascades with large  $m$  and  $z_{\text{max}}$  are relaxed.

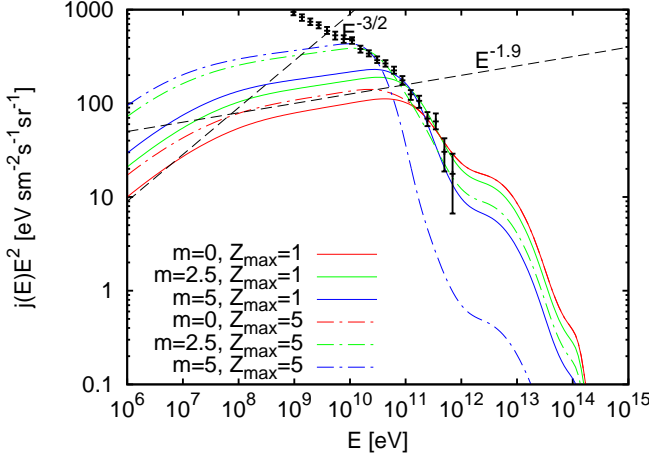


FIG. 10: Cascade spectra for source distribution (34), with  $E_s = 1$  PeV, with various  $m$  and  $z_{\max}$ , and with EBL model of Ref. [16]. The spectra are normalized by Fermi LAT EGB flux (with foreground model B) [7] shown by black errorbars.

We already have seen such effect in section II B for the case of analytic solution with the sharp high-energy cutoff, which starts at low energy (see Fig. 8) Now we can generalize the both cases formulating what will be called “ $E_{\max}$  rule” used here and below. It reads: *Increasing  $E_{\max}$  in the calculated cascade spectrum suppresses  $\omega_{\text{cas}}$ .* Indeed, Fig. 10 shows that increasing  $E_{\max}$  needs lowering the total curve  $J(E)$  to avoid the excess of predicted flux  $J(E)$  over the observed Fermi flux. For changing  $E_{\max}$  one may use, for example, the cosmological evolution: increasing  $z_{\max}$  results in decreasing  $E_{\max}$  at  $z = 0$  by factor  $(1 + z)$ .

Another feature observed in Fig. 10 is the standard energy spectra  $\propto E^{-1.5}$  transforming to  $\propto E^{-1.9}$  at higher energy (see these curves in the figure).

In Fig. 11 we present the maximum cascade energy density  $\omega_{\text{cas}}^{\text{iso}}$  consistent with Fermi IGRB flux and  $\omega_{\text{cas}}^{\text{tot}}$  consistent with Fermi EGB flux [7] for two cases of source distribution (33) and (34). To obtain these quantities we normalize the cascade spectrum calculated in numerical simulations by IGRB or EGB fluxes [7].

In the panel (a) we show the energy density  $\omega_{\text{cas}}^{\text{tot}}$  and  $\omega_{\text{cas}}^{\text{iso}}$  calculated in the model with fixed redshift of the source  $z_s$  and with fixed energy  $E_s$  of primary photon/electron. This is the case of strong universality, when the cascade spectrum is determined by single parameter  $\omega_{\text{cas}}$ . Uncertainties, caused by different EBL models are not large, and values of  $\omega_{\text{cas}}^{\text{tot}}$  are larger than  $\omega_{\text{cas}}^{\text{iso}}$ , as expected. The values of  $\omega_{\text{cas}}(z)$  at large  $z$  exceeds that at small  $z$  according to  $E_{\max}$  rule: large  $z$  gives small  $E_{\max}$ , small  $E_{\max}$  results in large flux, and hence in large  $\omega_{\text{cas}}$ . One can see this effect in Fig. 11a.

In Fig. 11b the case of more realistic continuous  $z$ -distribution, as given by Eq.(34), is presented. It is de-

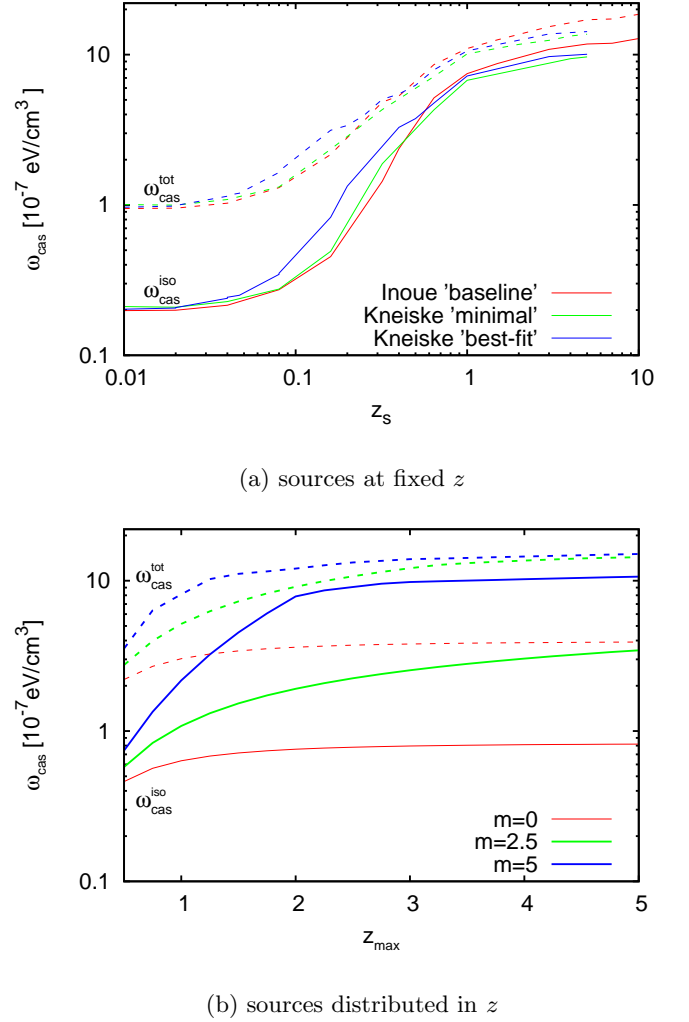


FIG. 11: Upper limits on the cascade energy density  $\omega_{\text{cas}}$  obtained for source distribution with fixed  $z_s$ , Eq. (33) (panel a), and with continuous  $z_s$  distribution, Eq. 34 (panel b). The total upper limits  $\omega_{\text{cas}}^{\text{tot}}$  are obtained using Fermi EGB flux (dashed lines) and isotropic upper limits  $\omega_{\text{cas}}^{\text{iso}}$  - using Fermi IGRB flux (full lines). The various EBL models are used in simulations shown in panel (a): Ref. [37] (red lines), Ref. [16] (blue lines), and Ref. [17] (green lines). In the lower panel (b) EBL model of Ref. [37] is used.

scribed by weak universality, when cascade spectrum depends, apart from  $\omega_{\text{cas}}$ , on other parameters, in particular on parameters of cosmological evolution  $m$  and  $z_{\max}$ . The low  $z$  and large  $z$  regimes exist here, too, being provided by  $E_{\max}$  rule.

The lowest  $\omega_{\text{cas}}^{\text{iso}} = 4 \times 10^{-8}$  eV/cm<sup>3</sup>, is obtained for  $z_{\max} \lesssim 1$  and for absence of evolution  $m = 0$ . It is an order of magnitude lower than the limit  $5.8 \times 10^{-7}$  eV/cm<sup>3</sup> found in [8] for the secondary photons produced during propagation of UHECR. The limit appears very restrictive for fluxes of protons in UHECR and cosmogenic neu-

trinos produced at  $z_{\max} \lesssim 1$  and in absence of evolution  $m = 0$ .

Non-evolutionary models with  $m=0$  and  $z_{\max} \gtrsim 2$  have  $\omega_{\text{cas}}^{\text{iso}} \leq 8 \times 10^{-8}$  eV/cm<sup>3</sup> (see Fig. 11 panel b) which allows some of non-evolutionary UHECR proton models from Table 1 of [36]. The models with strong evolution  $m = 5$  and  $z_{\max} \gtrsim 2$  allows large  $\omega_{\text{cas}}^{\text{iso}} \approx 8 \times 10^{-7}$  eV/cm<sup>3</sup> favourable for UHECR proton models with strong evolution and large  $z_{\max}$ .

The smallness of  $\omega_{\text{cas}}$  produced in cosmic ray models in comparison with  $\omega_{\text{cas}}^{\text{iso}}$  measured by Fermi LAT is not the only criterion for successful cosmic ray model. It must satisfy another more sensitive criterion: *not to exceed the Fermi IGRB flux in the highest-energy bin* (in fact this criterion enters the comparison of energy densities as integral characteristic). Unfortunately the IGRB flux estimate in the highest energy bin is strongly model dependent and suffers from low statistics. We have considered problem of survival of UHECR proton models in details in the separate work with emphasizing the role of the highest energy bin (in preparation). This problem was already studied in the works [8–10] and most recently in different approach in Ref. [49].

The above analysis is based on EGB and IGRB fluxes derived using 50 months of Fermi-LAT observation [7]. The two recent catalogs of observations which appear later [50] and [51] probably will change further our results. These catalogs are based on the new program of analysis, Pass 8, with the improved reconstruction and classification of events, and with the time of observation increased to 6 years. The analysis of the work [52] shows that the considerable fraction of high energy events above 50 GeV can be attributed to unresolved sources most of which are blazars. For EGB flux, contribution of blazars according to this work reaches  $86^{+16}_{-14}\%$ . This implies a stronger bound on the true isotropic flux. This effect can be roughly described by inequality

$$\omega_{\text{cas}}^{\text{iso}} \lesssim 0.28 \omega_{\text{cas}}^{\text{tot}} \quad (35)$$

## VI. SUMMARY

Using both analytic approach and numerical simulations we have described the development of electromagnetic cascades in the universe in presence of CMB and EBL background radiations. The cascades develop due to IC scattering on most numerous CMB photons  $e + \gamma_{\text{cmb}} \rightarrow e' + \gamma'$  and pair-production on less numerous EBL photons  $\gamma + \gamma_{\text{ebl}} \rightarrow e^- e^+$ . A primary particle below is called photon, though electron is implied under this name, too.

For analytic calculations we use *dichromatic model* with fixed energy of CMB photons  $\varepsilon_{\text{cmb}} = 6.3 \times 10^{-4}$  eV and EBL photons with  $\varepsilon_{\text{ebl}} = 0.68$  eV. In the cascade photon spectrum there are two characteristic energies: absorption energy  $\mathcal{E}_{\gamma}^{\text{ebl}} \sim m_e^2/\varepsilon_{\text{ebl}}$  and Inverse Compton energy of a photon  $\mathcal{E}_X = (1/3)(\mathcal{E}_{\gamma}/m_e)^2 \varepsilon_{\text{cmb}}$ , produced

by a born electron/positron in  $\gamma + \gamma_{\text{ebl}}$  collision. Thus in analytic dichromatic model we have:

$$\begin{aligned} \mathcal{E}_{\gamma}^{\text{ebl}} &= \frac{m_e^2}{\varepsilon_{\text{ebl}}} = 3.9 \times 10^{11} \text{ eV} \\ \mathcal{E}_X &= \frac{1}{3} \mathcal{E}_{\gamma}^{\text{ebl}} \frac{\varepsilon_{\text{cmb}}}{\varepsilon_{\text{ebl}}} = 1.2 \times 10^8 \text{ eV}. \end{aligned} \quad (36)$$

The cascade initiated at large distance by very high energy photon/electron has spectrum given by Eq. (9), which is  $\propto E^{-3/2}$  in low-energy regime  $E \lesssim \mathcal{E}_X$ , with  $\propto E^{-2}$  at intermediate energies  $\mathcal{E}_X \lesssim E \lesssim \mathcal{E}_{\gamma}$ , and with a high energy cutoff at  $\mathcal{E}_{\gamma}$ , where  $\mathcal{E}_{\gamma}$  numerically can differ from  $\mathcal{E}_{\gamma}^{\text{ebl}}$  in Eq. (36) due to different values of  $\varepsilon_{\text{ebl}}$ .

The numerical simulations confirm the analytic spectrum with index  $\gamma_1 = 3/2$  being exact,  $\gamma_2 = 2$  being approximate ( $\gamma_2 \approx 1.9$  in numerical simulations) and with a sharp high-energy cutoff for a source at very large distance. The artificially sharp energy transitions in analytic spectrum at  $E = \mathcal{E}_X$  and  $E = \mathcal{E}_{\gamma}$  appear in numerical simulations as continuous transition features. This is most important difference between analytic solution and more precise numerical simulation.

The remarkable feature found in both analytic and numerical solutions is *universality* of the cascade spectrum. In analytic solution the strong universality is seen explicitly from the spectrum given by Eq.(9), where the shape of the spectrum does not depend on initial energy of the primary photon at  $E_s > E_0$ , and on distance to observer  $r$ , unless it is too small. The energy scale of universality is  $E_0 = \mathcal{E}_{\gamma}^{\text{cmb}} = 0.4$  PeV. The energy  $\mathcal{E}_X$  which separates two regimes,  $\propto E^{-3/2}$  and  $\propto E^{-2}$ , and energy of spectrum cutoff  $\mathcal{E}_{\gamma}$  are build from the main physical constants of the model (see Eq. (5)) and the cascade energy spectrum does not depend on variables of the model, in particular on initial energy  $E_s$  and distance to the source  $r$ . The main features of this universality, specific for analytic model developed in section II A, are: (i) the same energy shape of the cascades produced by primary photon/electron if its energy  $E_s$  is larger than universality scale  $E_0$ , (ii) the same cascade energy spectrum for any injection spectrum  $Q(E)$  at  $E \geq E_0$  (in other words cascade spectrum forgets what injection spectrum produced it), (iii) independence of spectrum shape from distance to the point where cascade started, and (iv) energy density of the cascade  $\omega_{\text{cas}}$  as the only cascade parameter which determines the spectrum shape.

These properties of 'analytic' cascades are referred to as *strong universality*.

For realistic cascades in the expanding universe, property (i) is modified as follows: cascades initiated at the fixed redshift  $z$  by photon/electron with sufficiently high energy  $E_s > E_0$  turn at  $z = 0$  into cascades with spectrum independent of  $E_s$  but dependent on  $z$ . These spectra are calculated by numerical simulation. Property (ii) remains almost the same: cascade spectra initiated at the same  $z$  with different injection spectra  $Q(E)$  are almost identical. However, if injection spectrum  $Q(E, z)$

smoothly changes with  $z$  the total diffuse spectrum obtained by integration over  $z$  is not universal; the spectra are different for different dependence of  $Q(E, z)$  on  $z$ . The diffuse spectra for various  $Q(E, z)$  are determined in this case not only by  $\omega_{\text{cas}}$  but also by other parameters from  $Q(E, z)$  distribution.

We refer to the case described above as *weak universality*. Some of the described properties of these cascades, studied in numerical simulations are shown in Fig. 9.

The main aim of this paper is to obtain the upper limit on the cascade energy density  $\omega_{\text{cas}}$  using the Fermi LAT flux of gamma radiation. In the analytic model with strong universality, there is the direct and transparent method which allows us to obtain strong enough upper limit on the cascade energy density. This upper limit follows from Eq. (29) and results in  $\omega_{\text{cas}} \leq 8.3 \times 10^{-8} \text{ eV/cm}^3$ . The specific property of this limit is the high-energy cutoff, i.e.  $E_{\text{max}}$ , given by  $\mathcal{E}_\gamma = m_e^2/\varepsilon_{\text{ebl}}$ , which at  $\varepsilon_{\text{ebl}} \sim 1$  eV coincides with cutoff energy in Fermi IGRB spectrum. The limit is stronger if the model-dependent  $E_{\text{max}} = \mathcal{E}_\gamma$  is higher.

Even more stronger upper limit is obtained comparing the *numerical calculations* of the cascade energy shape with the Fermi measured spectrum, due to its high-energy tail. If the calculated spectrum crosses the steep high-energy Fermi tail at  $E_{\text{cross}}$ , the calculated flux above  $E_{\text{cross}}$  exceeds the observations. To eliminate this contradiction one must lower the total calculated spectrum decreasing  $\omega_{\text{cas}}$ , and thus we arrive at “ $E_{\text{max}}$ -rule” formulated in subsection VB as: “Increasing  $E_{\text{max}}$  in the calculated spectrum suppresses further  $\omega_{\text{cas}}$ .”

In particular,  $E_{\text{max}}$ -rule works efficiently in evolutionary  $(1+z)^m$  models with large  $m$  and large  $z_{\text{max}}$ . Since the flux in these models is dominated by production at  $z_{\text{max}}$ , the maximum energy  $E_{\text{max}}$  at  $z = 0$  becomes  $(1+z_{\text{max}})$  times less and respectively  $\omega_{\text{cas}}$  is allowed to be higher, as one observes in Fig. 11b.

We describe now the obtained limits on  $\omega_{\text{cas}}$  in some details.

Fermi LAT presented two kinds of measured extragalactic fluxes: the total Extragalactic Background flux (EGB) and Isotropic Gamma Ray Background flux (IGRB). The corresponding energy densities obtained, using EGB and IGRB as the upper limits, are  $\omega_{\text{cas}}^{\text{tot}}$  and  $\omega_{\text{cas}}^{\text{iso}}$ , respectively, the former being always larger. Both fluxes, EGR and IGRB, have systematic and statistical uncertainties, and are to some extent model dependent (e.g. foreground models). To be conservative we use maximal fluxes allowed within these uncertainties.

The both spectra, EGR and IGRB, have steepening, which starts at  $E_{\text{cut}} = 250$  GeV and at higher energies become steeper. The method of  $\omega_{\text{cas}}$  calculation is mainly

based on this steep high energy feature.

The shape of the cascade spectrum is accurately calculated using kinetic equations and MC methods. As these calculations show,  $E_{\text{max}}$  in the cascade spectrum at  $z = 0$  becomes smaller at larger  $z_s$  of cascade production. Since flux of EGR/IGRB is  $J(E) \propto E^{-3.2}$ , small  $E_{\text{max}}$  results in larger flux  $J(E_{\text{max}})$ , i.e. in larger  $\omega_{\text{cas}}$ . In other words  $\omega_{\text{cas}}$  is rising with increasing  $z_s$  as we see indeed in Fig. 11a.

Fig. 11a show the case of fixed  $z_s$ , when strong universality holds and thus  $\omega_{\text{cas}}$  value is unique for each  $z_s$ . As expected  $\omega_{\text{cas}}^{\text{tot}}$  is larger than  $\omega_{\text{cas}}^{\text{iso}}$ . For small distances  $z_s < 0.1$  cascades are underdeveloped and  $\omega_{\text{cas}}$  are small:  $\omega_{\text{cas}}^{\text{iso}} \lesssim (2-3) \times 10^{-8} \text{ eV/cm}^3$ . At large  $z_s \gtrsim 1$  energy density is larger:  $\omega_{\text{cas}}^{\text{iso}} \gtrsim (5-8) \times 10^{-7} \text{ eV/cm}^3$ . These results depend weakly on models of EBL.

The strong dependence of  $\omega_{\text{cas}}$  on redshift  $z_s$  in Fig. 11a implies dependence of energy density on source distribution over  $z$ , seen in Fig. 11b. One may observe there an increase of  $\omega_{\text{cas}}$  with  $z_{\text{max}}$  up to  $z_{\text{max}} \sim 1$ , with the constant value at larger  $z_{\text{max}}$ . This constant value depends on cosmological evolution  $(1+z)^m$ . One may summarize the values of  $\omega_{\text{cas}}^{\text{iso}}$  as  $5 \times 10^{-8} \text{ eV/cm}^3$  in the case of absence of cosmological evolution  $m = 0$  and up to  $9 \times 10^{-7} \text{ eV/cm}^3$  in case of strong cosmological evolution  $m = 5$ .

The large  $\omega_{\text{cas}}^{\text{max}}$  allowed in case of strong evolution with large  $z_{\text{max}}$  is explained by diminishing of  $E_{\text{max}}$  by factor  $(1+z)$  in the cascade spectrum at  $z = 0$ .

The first results of Fermi LAT [6] demonstrated [8–10] that cascade energy density  $\omega_{\text{cas}} \approx 5.8 \times 10^{-7} \text{ eV/cm}^3$  excludes some proton models of UHECR and cosmogenic neutrinos. However, some models survived. The new data of Fermi LAT [7] discovered the steep energy feature in the end of the spectrum which further constraints the cascade energy density. The new limit is model-dependent. For models with strong universality of cascade spectrum the limits on  $\omega_{\text{cas}}$  became stronger and restrictions on UHECR became more severe. However, for the models with weak universality the restrictions relaxed. In particular, the evolutionary models with strong evolution and large  $z_{\text{max}}$  the energy density can be larger than  $6 \times 10^{-7} \text{ eV/cm}^3$ , i.e. larger than previous limit.

*Acknowledgments*—Numerical calculations have been performed at the computer cluster of the Theoretical Physics Division of the Institute for Nuclear Research of the Russian Academy of Sciences with support by the Russian Science Foundation, grant 14-12-01340. OK is grateful to GSSI and LNGS for hospitality.

- 
- [1] A. A. Penzias, R. W. Wilson Ap. J. **142**, 419 (1965).  
 [2] K. Greisen, Phys. Rev. Lett. **16**, 748 (1966); G. T. Zat-

- sepin and V. A. Kuzmin, XCyJETP Lett. **4**, 78 (1966)  
 [Pisma Zh. Eksp. Teor. Fiz. **4**, 114 (1966)].



- [3] V. S. Beresinsky and G. T. Zatsepin, Phys. Lett. B **28**, 423 (1969); Sov. J. Nucl. Phys. **11**, 111 (1970).
- [4] V. S. Berezinsky and A. Yu. Smirnov, Astrophys. Sp. Sci. **32** 461 (1975).
- [5] P. Sreekumar et al., Ap. J., **494**, 523 (1998).
- [6] A.A.Abdo et al Fermi-LAT Collaboration, Phys Rev Lett. **104**, 101101 (2010).
- [7] M. Ackermann *et al.* [Fermi-LAT Collaboration], Astrophys. J. **799**, no. 1, 86 (2015) [arXiv:1410.3696 [astro-ph.HE]].
- [8] V. Berezinsky, A. Gazizov, M. Kachelrieß, S. Ostapchenko, Phys. Lett. B **695**, 13 (2011), arXiv:1003.1496.
- [9] M. Ahlers, L.A. Anchordoqui, M.C. Gonzalez-Garcia, F. Halzen, S. Sarkar. Astropart. Phys. **34**, 106 (2010), arXiv:1005.2620
- [10] G.B. Gelmini, O. Kalashev, D.V. Semikoz, JCAP **1201**, 044 (2012), arXiv:1107.1672
- [11] O. F. Prilutsky, PhD thesis from Moscow Engineering Institute, 1972.
- [12] A. W. Strong, A. W. Wolfendale, J. Wdowczyk, Nature **241**, 109 (1973).
- [13] R. J. Gould and D. Schreder, Phys. Rev. Lett. **16**, 252 (1966).
- [14] V. S. Berezinsky, Soviet Physics: Nuclear Physics **11**, 399 (1970) (preprint P.N. Lebedev Institute of Physics, May 1969).
- [15] F. A. Aharonian, P. S. Copi, H. J. Völk, Ap. J. Lett **423**, L5 (1994).
- [16] T. M. Kneiske et al., Astron. Astrophys. **386**(2002) 1; *ibid.*, **413** (2004) 807.
- [17] T. M. Kneiske and H. Dole, arXiv:1001.2132 [astro-ph.CO].
- [18] A. Neronov, D. V. Semikoz, JETP Letters **85**, 579 (2007), arXiv:astro-ph/0604607.
- [19] P. P. Kronberg, Reports Progress Physics **57**, 325 (1994).
- [20] D. Grasso, H. R. Rubinstein, Phys. Rep. **348**, 163, (2001).
- [21] R. M. Kulsrud, E. G. Zweibel, Reports in Progress of Physics **71**(4) 046,901 (2008). 0707.2783
- [22] R. Durrer and A. Neronov, Astron. Astrophys. Rev. **21**, 62 (2013) [arXiv:1303.7121 [astro-ph.CO]].
- [23] L. Biermann, Z.Naturforsch. **5a**, 65 (1950)
- [24] L. Mestel, D. L. Moss,
- [25] M. V. Medvedev, A. Loeb, Ap.J. **526**, 697 (1999).
- [26] F. Miniati, A. R. Bell, Ap.J. **729**, 73 (2011).
- [27] A. Elyiv, A. Neronov, D. V. Semikoz. arXiv:0903.3649[astro-ph.CO]
- [28] A. Neronov, L. Vovk. Science, **328**, 73 - 75 (2010), arXiv:1006.3504 [astro-ph.HE].
- [29] A. M. Taylor, I. Vovk and A. Neronov, Astron. Astrophys. **529**, A144 (2011) [arXiv:1101.0932 [astro-ph.HE]].
- [30] H. Tashiro, W. Chen, F. Ferrer, T. Vachaspati, Month. Not. R. Astro. Soc. **445**, L41 (2014).
- [31] W. Chen, B. D. Chowdhury, F. Ferrer, H. Tashiro, T. Vachaspati, arXiv:1412.3171 [astro-ph.CO].
- [32] V. Berezinsky, Yad. Fiz. **11**, 399 (1970).
- [33] G. R. Blumenthal and R. J. Gould, Reviews of Modern Physics **41**, 237 (1970).
- [34] V. S. Berezinsky, S. V. Bulanov, V. A. Dogiel, V. L. Ginzburg and V. S. Ptuskin, Astrophysics of Cosmic Rays (Elsevier, Amsterdam (1990), originally in Russian, Nauka (1984).
- [35] M. Kachelrieß, S. Ostapchenko and R. Tomas, Comput. Phys. Commun. **183**, 1036 (2012) [arXiv:1106.5508 [astro-ph.HE]].
- [36] V. Berezinsky, A. Gazizov, M. Kachelrieß, S. Ostapchenko, Phys. Lett. B **695**, 13 (2011).
- [37] Y. Inoue et al., arXiv:1212.1683.
- [38] O. K. Kalashev, PhD thesis, Institute for Nuclear Research RAS, Moscow 2003. O. E. Kalashev and E. Kido, arXiv:1406.0735 [astro-ph.HE].
- [39] G. B. Gelmini, O. Kalashev and D. V. Semikoz, JCAP **1201**, 044 (2012).
- [40] S. Lee, Phys. Rev. D **58**, 043004 (1998) [astro-ph/9604098].
- [41] S. Yoshida, G. Sigl and S. -j. Lee, Phys. Rev. Lett. **81**, 5505 (1998) [hep-ph/9808324].
- [42] J. R. Primack, R. C. Gilmore and R. S. Somerville, AIP Conf. Proc. **1085**, 71 (2009); J. D. Finke, S. Razzaque and C. D. Dermer, Astrophys. J. **712**, 238 (2010).
- [43] A. Franceschini, G. Rodighiero and M. Vaccari, Astron. Astrophys. **487**, 837 (2008) [arXiv:0805.1841 [astro-ph]].
- [44] F. W. Stecker, M. A. Malkan and S. T. Scully, Astrophys. J. **648**, 774 (2006).
- [45] F. W. Stecker, M. A. Malkan and S. T. Scully, Astrophys. J. **761**, 128 (2012). S. T. Scully, M. A. Malkan and F. W. Stecker, arXiv:1401.4435 [astro-ph.HE].
- [46] W. Essey, O. Kalashev, A. Kusenko and J. F. Beacom, Astrophys. J. **731**, 51 (2011).
- [47] A. A. Abdo *et al.* Astrophys. J. **723**, 1082 (2010).
- [48] For a standard textbook discussion, see J. D. Jackson, *Classical Electrodynamics*, 2nd Ed. (John Wiley & Sons, New York, 1975).
- [49] R. Y. Liu, A. M. Taylor, X. Y. Wang and F. A. Aharonian, arXiv:1603.03223 [astro-ph.HE].
- [50] F. Acero *et al.* [Fermi-LAT Collaboration], arXiv:1501.02003 [astro-ph.HE].
- [51] M. Ackermann *et al.* [Fermi-LAT Collaboration], Astrophys. J. Suppl. **222**, no. 1, 5 (2016) doi:10.3847/0067-0049/222/1/5 [arXiv:1508.04449 [astro-ph.HE]].
- [52] M. Di Mauro [Fermi-LAT Collaboration], arXiv:1601.04323 [astro-ph.HE].